The meridional and seasonal variability of the carbonate system in the Southeast Atlantic sector of the Southern Ocean: SCALE 2019 Experiment

Student number: BNSZAN001

Supervisor: Dr. Pedro Monteiro

Table of Contents

Table of figures

List of abbreviations

AAIW: Antarctic Intermediate Water

AASW: Antarctic Surface Water

ACC: Antarctic Circumpolar Current

A_T: Total Alkalinity

$CaCO_3$: Calcium Carbonate

CRM: Certified Reference Material

CO_2 : Carbon Dioxide

CRM : Certified Reference Material

CTD : Conductivity, Temperature and Depth

C_T : Dissolved Inorganic Carbon

ESACW: Eastern South Atlantic Central Water

fCO_2 : Fugacity of carbon dioxide

GT : GoodHope Transect

LIAR: Locally Interpolated Alkalinity Regression

MIZ : Marginal Ice Zone

OA : Ocean Acidification

pCO_2 : Partial Pressure of Carbon Dioxide

PFZ: Polar Front Zone

PUZ : Polar Upwelling Zone

RF : Revelle Factor

SACCF: Southern Antarctic Circumpolar Current Front

SAF: Subantarctic Front

SAMW: Subantarctic Mode Water

SAZ : Sub-Antarctic Zone

SBdy: Southern Boundary of Antarctic Circumpolar Current

SLA: Sea Level Anomaly

SO : Southern Ocean

SSS: Sea Surface Salinity

SST: Sea Surface Temperature

STF: South Subtropical Front

UCDW: Upper Circumpolar Deep Water

VINDTA : Versatile INstrument for the Determination of Titration Alkalinity

WS : Whale Survey

WW: Winter Water

Abstract

Unlike well-characterized regions that have emerging pH and carbonate data, distant areas like polar oceans remain seasonally undersampled. Consequently, there may be a significant gap in our understanding of biological implications of future ocean acidification (OA). This study seeks to examine the seawater state conditions of the carbonate system that are currently experienced by marine organisms that depend on pH and Aragonite saturation (Ω_{Ar}) for calcification. The main focus was on how the physical and carbonate characteristics are sensitive to seasonal variability in the S.E Atlantic sector of the Southern Ocean. We analyzed the temperature, salinity, Dissolved Inorganic Carbon (C_T), alkalinity data (A_T), pH and Omega (Ω_{Ar}) at the surface and in the upper 1000m. We then compared the seasonal meridional gradients in the surface layer and in the upper 1000m water column. The C_T and A_T were measured using a VINDTA instrument while pH and Ω_{Ar} were derived using the CO_2SYS program. The initial hypothesis was that the southernmost part of the Southern Ocean would acidify more in winter than in spring. This was based on the idea that colder waters hold more CO_2. However, we found remarkable results showing that the surface C_T was consistently higher in spring than in winter, with mean seasonal differences ranging from 5.86-21.90µmol/kg although SST was consistently higher in spring than winter, with mean seasonal differences ranging from 0.67-2.12˚C within the ocean front boundaries. It was then hypothesized that the temperature, biological production and CO_2 flux seasonal cycles may have been out of phase. Consistent with the C_T gradient, the surface pH and Ω_{Ar} were ±0.05 units lower in the warmer waters of spring and comparatively higher in winter. The seasonal lag was seen even within the interior layers of the column. There were three main findings in this study: Firstly, since the biogeochemically controlled seasonal CO_2 seasonal transition variability lagged the heat flux influence on SST, the expected winter and spring seasonal conditions for carbonate were not reflected in the timing of the winter and spring cruises. Secondly, we observed an uncoupling of pH and ΩAr surface meridional gradients. While pH had no significant meridional gradient trend apart from frontal variability, ΩAr followed the meridional trend that was driven by C_T. This was due to the impact of the meridional temperature gradient on K_2 that compensated for the impact of the C_T gradient on the pH. Lastly, we found that the impact of the seasonal cycle of carbonate stretched down to 1000 m and it was attributed to physical processes. Our findings led us to infer that from a carbonate perspective, the winter cruise was in fact the tail end of autumn while the spring cruise was the tail end of winter.

1. Introduction

1.1 Problem statement

The Southern Ocean has long been recognized as playing an important role in the biological productivity and in the global carbon cycle (Sarmiento and Gruber, 2006). The surface of the ocean covers over 70% of our planet and only 30% of this is made up of the Southern Ocean south of 30°S, yet it is responsible for sinking about 43 percent of CO_2 that comes from anthropogenic sources (Williams *et al.*, 2018). CO_2 concentrations in the atmosphere have been reduced by the ocean's absorption of at least 25% of all anthropogenic CO_2 each year since the industrial revolution (Ishii *et al.*, 2011). This comes with detrimental impacts because it causes significant alterations in seawater chemistry, the carbonate system in particular (Stark *et al.*, 2018). The carbonate system is responsible for acid-base buffering of seawater (Bustos-serrano, 2010).

The availability of nutrients in organisms may be compromised by OA (Cao and Caldeira, 2008). For instance, Iron is a limiting nutrient in the Southern Ocean (Andrew *et al.*, 2019) and since it is highly sensitive to pH, OA affects its availability to phytoplankton (Shi *et al.*, 2010). Antarctic waters in particular have very few observations of temporal and spatial variation of carbonate chemistry (Stark *et al.*, 2018) so there is a lack of understanding of the seasonality of the carbonate system which is necessary to explain and project OA. Alterations in seawater chemistry also affect coccoliths which are are calcium carbonate platelets that become suspended in the water column after detaching when coccolithophores bloom (Mitchell *et al.*, 2017). It was discovered that the declining concentration of carbonate ions led to a decrease in coccolith mass, and this was found to have some spatiotemporal consistency (Beaufort *et al.*, 2011;Riebesell *et al.*, 2013).

1.2 Potential impact of this study

Historically, the Southern Ocean CO_2 is under sampled and seasonally biased towards summer (Gregor, 2019; Gray, 2018). Although there is a large number of observations available in the Southern Ocean, the data are temporally and spatially concentrated, with summer seasonal biases. Large bands of the Southern Ocean are completely unsampled because most data are collected on repeat hydrographic lines or during reoccupations of supply routes to Antarctic bases (Gray, 2018). Since the available data sets tend to be biased towards coastal data and summer, the seasonal cycles

in carbonate system parameters are often underestimated because even the most realistic Earth system models tend to both underestimate the seasonal cycles in carbonate system parameters and be biased (Mongwe *et al.*, 2018). Reason being data sets that exist are often biased toward summer or heavily weighted towards data from the Drake passage (Williams *et al.*, 2018). This setback might be alleviated in this study as the knowledge of the present-day pH dynamics in the ocean would give us insight into current day physiological stress on species and how they might be resilient to future OA conditions. Models and other observations have shown contrasting seasonal cycle responses of the two commonly used OA metrics, Ω_{Ar} and pH to C_T increases throughout the global surface ocean, suggesting that the intensification of seasonal variability may be more rapid on cold high latitude margins and upwelling-dominated regions since they are highly sensitive to increasing CO_2 content and have naturally lower buffering capacity (Cai *et al.*, 2020).

Changes in ocean uptake of carbon dioxide through changes in carbonate buffering capacity that can influence future climate change trajectories will be understood better. A better understanding of changes in seawater pH and Ω_{Ar} will also be useful for managing the socioeconomic and ecological consequences of OA (Mitchell *et al.*, 2017). A better characterization of natural variability in carbonate chemistry will also assist manipulative field experiments with planning and interpretation of related experimental results (Stark *et al.*, 2018). Furthermore, the observations of how ocean conditions are changing on the spatiotemporal scale are needed to constrain the uptake of carbon, its rate of storage and the consequential impacts in the ecosystem (Bushinsky, Takeshita and Williams, 2019).

This study is a unique study investigating the seasonal meridional contrasts between winter and spring-summer periods in the South East Atlantic Ocean both at the surface and in the upper 1000 m. In order to understand the seasonal variability of the carbonate system here I examine the seasonality of the carbonate system.

1.3 Rationale and literature review

Here we start by explaining how the CO_2 invades the Southern Ocean and then we look into the equilibrium shift of the carbonate system as the consequence of that CO_2 invasion.

1.3.1 The invasion of CO_2 in the Southern Ocean and the equilibrium shift

Chemically, the invasion of anthropogenic CO_2 is said to be equivalent to adding carbonic acid into seawater and this addition of carbonic acid elevates the concentration of hydrogen ions (Ishii *et al.*, 2011) thus decreasing the pH (ocean acidification). Even with this decline in pH, on average, the pH of the surface waters does not differ much from what it was before, despite the increase in atmospheric CO_2 concentrations. This was attributed to the buffering process as the seawater interacts with sediments that are rich in calcium carbonate ($CaCO_3$) (Coughlan, 2013). The uptake of CO_2 comes at a cost of Carbonate ions (Equation 1) while making two bicarbonate ions.

$$CO_2 + H_2O + CO_3^{2-} \Longleftrightarrow 2HCO_3^- \quad (1)$$

Henry's law states that there is a directly proportional relationship between the solubility of a gas and the partial pressure in the overlying air (Murray, 2004). Following Henry's law, the flux of CO_2 into the ocean increases with the increase of the atmospheric concentration of this gas (Coughlan, 2013). As the atmospheric pCO_2 increases, the C_T will also increase, shifting the equilibrium of the carbonate system to greater levels of CO_2 and lower pH (Figure 1).

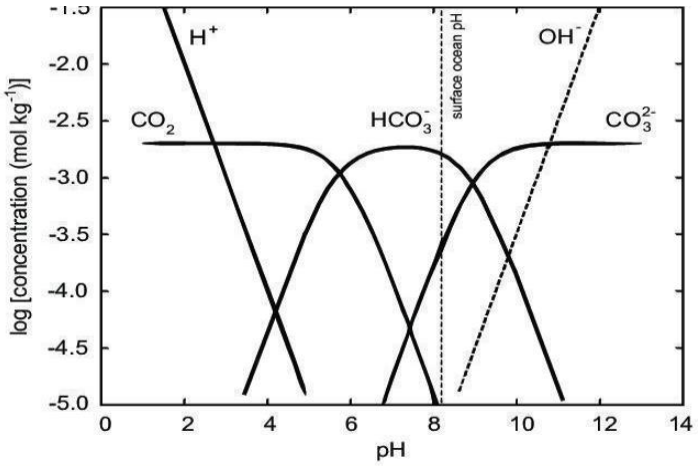

Figure 1: Bjerrum plot showing showing the pH dependent equilibration of carbon species concentration i.e the the pH decrease as H^+ and CO_2 concentrations increase (Henriet *et al.*, 2015).

1.3.2 Changes in carbon species and carbonate parameters

The carbonate parameters that we will investigate in this study are A_T, C_T, and the pH.

1.3.2.1 The A_T

The alkalinity moderates the process of the resulting decline in pH and carbonate concentration (Coughlan, 2013). This project will examine how the effects of the uptake of oceanic CO_2 are buffered by the ocean by exploring changes in carbonate parameters. The definition of A_T is complex as it is as much of a concept as it is precisely quantitative. Total Alkalinity is most simply expressed in terms of the quantity of protons from strong acids needed to titrate seawater to a pH of 4.3 (Murray, 2004), also known as titration alkalinity. The alkalinity end point is reached at this pH (Figure 2) and the proton balance is achieved where the H^+ and HCO_3^- ions are equal at this point. In addition to carbon species, additional acid/base species are also reflected (Equation 2) (Byrne, 2014). Some constituents are so small in amounts that their impact is negligible (Dickson, Sabine and Christian, 2007).

$$A_T = [HCO_3^-] + 2[CO_3^{2-}] + [B(OH)_4^-] + [OH^-] - [H^+] + \text{minor constituents} \quad (2)$$

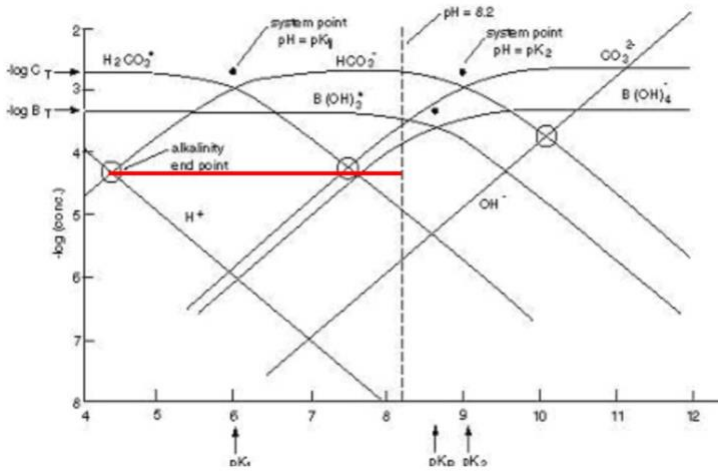

Figure 2: The Bjerrum plot shows the decrease in pH from about 8.2 to about 4.3 when seawater is titrated by a strong acid (shown by a solid red line) (Zeebe and Wolf-Gladrow, 2009). Seawater constants are shown by the arrows in the x-axis.

1.3.2.2 The Dissolved Inorganic Carbon (C_T)

The sum of the total concentrations of carbonate species (Equation 3) is defined as the dissolved Inorganic Carbon (C_T).

$$C_T = [CO_2^*] + [HCO_3^-] + [CO_3^{2-}] \quad (3)$$

The concentration of the hypothetical, aqueous species CO_2^* is the sum of the concentrations of the unionized species $CO_2(aq)$ and $H_2CO_3(aq)$ (Dickson, 2010).

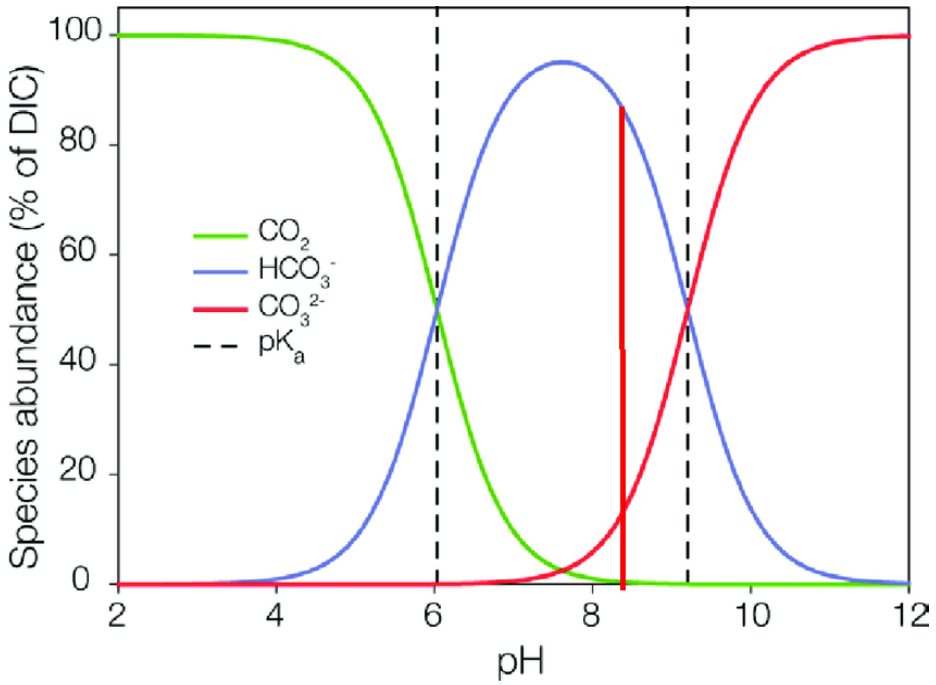

Figure 3: Bjerrum plot (Rokitta, 2012) showing the relative abundance of C_T species at seawater pH of 8.2 which is shown by the red vertical line. pKa is the pK value of an acid.

With the current pH of about 8.2, approximately 1% of the C_T is in the form of aqueous CO_2 which includes minute amounts of carbonic acid. The most abundant species are bicarbonate ions which make up about 90% of C_T (Figure 3). The rest is in the form of carbonate ions which are about 9% (Coughlan, 2013). These abundances change with varying salinity, temperature and pressure and they are a reflection of the pH because pH is a master variable of the carbonate system (Murray, 2004).

1.3.2.3 The pH scale

$$pH = -\log [H^+] \quad (4)$$

The pH is defined as the negative log of the total hydrogen ion concentration (Equation 4) where a total scale is used to express the concentration of hydrogen ions (Dickson, 2010). It is used to assess the carbonate equilibrium of the ocean directly (Byrne, 2014). As a weak acid, the CO_2 concentration is inversely proportional to the pH. The total hydrogen ion concentration scale (pH_T) will be used to calculate pH at a constant temperature of 25˚C (pH, $_{25}$). It is different from other pH scales in that it takes into account the effect of sulfate ions (Dickson, 2010). Total hydrogen ion scale is defined as $[H+] = [H+]_F (1+ S_T / K'_S)$ where S_T is the total amount of sulfate ion present in the seawater (Dickson, 2010). The total stoichiometric concentration of a species is the sum of the concentrations of the free species itself, together with the concentrations of all complexes that are formed between that species and the components of the ionic medium. In the case of hydrogen ion, such complexes occur with water (there are no unhydrated protons present in aqueous solution), and with sulfate ion to form the hydrogen sulfate anion: HSO^-_4 (Dickson, 2010). At all times, the chosen equilibrium constants should be the ones that are defined on that same pH scale used (Dickson, 2010) ; otherwise systematic errors arise when calculating the pH.

1.3.3 Buffering the ocean pH

With the various changes to properties of seawater, the chemical buffer by carbonate species is still efficient (Zeebe and Wolf-Gladrow, 2009). For instance, volcanism may naturally add hydrochloric acid into seawater and the carbonate system would buffer the addition of this strong acid. The concentrations of hydrogen and chloride ions would be expected to increase in a ratio of 1:1 in a solution of distilled water when HCl is added. The seawater behaves differently. For instance, the pH of distilled water would decrease from 7 to 6 if 1 µmol/kg of HCl was added. The pH would only drop to 6.997 when the same amount is added to seawater with the temperature of 15˚C, salinity of 35, C_T of 2000µmol/kg and the pH of 7 (Zeebe and Wolf-Gladrow, 2009). The pH would only drop from 7 to 6.9 in seawater as opposed to dropping from 7 to 6 in distilled water because of the capacity of carbonate and bicarbonate species to accept protons in seawater thus providing an efficient chemical buffer to various processes that change the seawater properties (Zeebe and Wolf-Gladrow, 2009). The ability of bicarbonate ions and carbonate ions to accept protons result in this buffering of seawater pH. When carbonate ion concentration decreases as CO_2 uptake is enhanced, the saturation state (Ω) will also decrease since they are proportional (equation 5- a simplified form of the $CaCO_3$ equilibrium equation).

An example of submarine volcanism can be found in the study that was conducted in Hawaii at the shoreline of Kilauea Volcano. During this study, they observed that when seawater and lava made contact, large amounts of acid were created and the decrease in the pH of seawater arised from the direct venting of magmatic CO_2 and to a lesser degree from magmatic SO_2 with minor additions from HF and HCl (Resing and Sansone, 1999).

1.3.4 Changes in the saturation state

$$\Omega = [Ca^{2+}][CO_3^{2-}]/K_{sp} \quad (5)$$

Where Ksp represents the solubility products of aragonite or calcite.

The OA lowers the concentration of carbonate ions to the point where calcium carbonate shells start to dissolve when K_{sp} is less than one (McNeil and Matear, 2008). Aragonite and calcite saturation states that are less than one are indices of thermodynamic tendency for dissolution but when these two are greater than one they become indices of thermodynamic tendency for precipitation (Raimondi *et al.*, 2019). Thus, the ocean is said to be supersaturated when Ω is greater than one, which causes Ω to be preserved and it is undersaturated when Ω is less than one since that signifies $CaCO_3$ dissolution (Byrne, 2014).

The saturation horizon is the depth where Ω is equal to one (Byrne, 2014). The saturation horizon is mostly set by the C_T and A_T profiles and solubility of $CaCO_3$ increases with the increase in pressure and declining temperature. It is the depth where biogenic $CaCO_3$ is well-preserved (K_{sp} >1) ; the seawater above this depth is supersaturated while the water underneath it is undersaturated (Coughlan, 2013). Currently, carbonate minerals tend to be preserved due to super-saturation in much of the surface waters. Contrary to this, most deep waters are undersaturated, mineral forms of $CaCO_3$ dissolve under these conditions. Since calcite is less soluble in comparison to aragonite, the saturation horizon of aragonite is thus closer to the surface than that of calcite. As a result of $CaCO_3$ production, the amount of alkalinity that is removed from seawater is twice as much as the amount of C_T that is removed. The pCO_2 thus becomes elevated at the surface with the decrease in $CaCO_3$. $CaCO_3$ and particulate organic carbon cycles offset each other in respect of pCO_2. On the other hand, the export of carbon to the bottom of the ocean will be reduced as the ratio of $CaCO_3$ to particulate organic carbon declines (Coughlan, 2013). The other processes responsible for changes in carbonate chemistry are explained below.

1.3.5 Processes that alter the carbonate chemistry in the Southern Ocean

In a study that was conducted in the Southern Ocean by Williams and others (2018), a decrease in A_T/C_T, pH and Ω was shown as you move poleward while C_T and pCO_2 increased at 200m. This was attributed to upwelling of the C_T -rich water in the southernmost regions. In the zones where wintertime mixed layers can reach 200m or deeper (SAZ,PFZ and ASZ) the seasonal cycle was distinguishable at 200m in most parameters (Williams *et al.*, 2018). As CO_2 from the atmosphere invades the seawater parcel, the C_T increases while the release of CO_2 results in decreased C_T levels as shown in Figure 4 (Zeebe and Wolf-Gladrow, 2009).

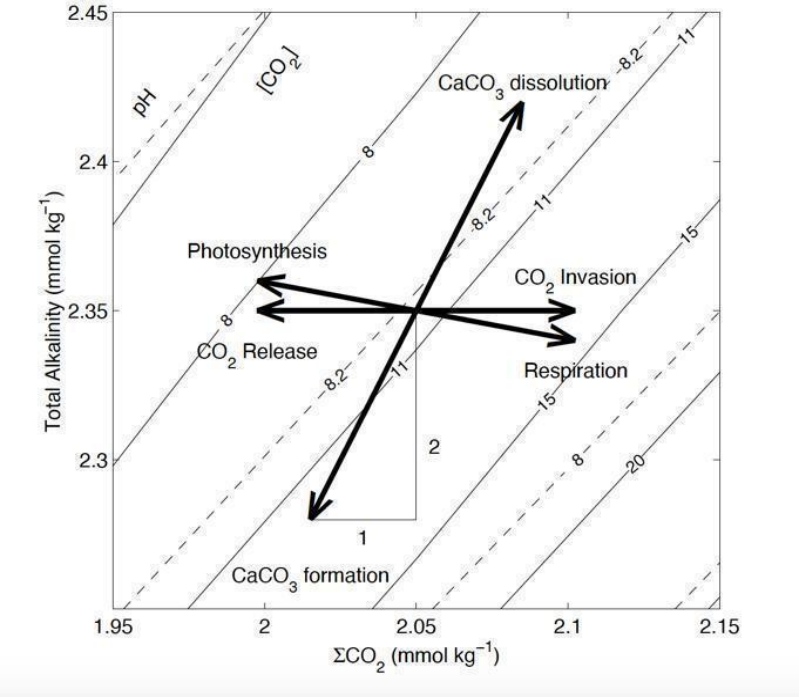

Figure 4: The processes that change concentrations of A_T and C_T in the ocean (Zeebe and Wolf-Gladrow, 2009).

Adding CO_2 to seawater has no direct effect on the A_T so it stays the same (Byrne, 2014). The air-sea exchange of CO_2 does not alter A_T because the definition of A_T as seen in equation 2 comprises a proton balance and the concentrations of conservative ions or charged chemical species are not affected by the release or invasion of CO_2 (Rokitta, 2012; Sarmiento and Gruber, 2006; Dickson, 2010). The trend of photosynthesis and respiration is similar to that of the removal and invasion of CO_2 (Figure 4), except that the nutrients slightly change the A_T when they are being released or taken up (Zeebe and Wolf-Gladrow, 2009). The ratio of A_T and C_T decreases by 2:1 during $CaCO_3$ precipitation and dissolution, this causes the concentration of CO_2 to increase regardless

of the decline in inorganic carbon (Zeebe and Wolf-Gladrow, 2009). Equation 6 shows that CO_2 is released when $CaCO_3$ gets precipitated.

$$Ca^{2+} + 2HCO_3^- \rightarrow CaCO_3 + CO_2 + H_2O \quad (6)$$

Due to the effect of buffering, one mole of precipitated CaCO3 does not increase the concentration of CO_2 by one mole. Rather, both the buffer capacity of seawater as well as the decrease of *A*T and C_T in a ratio of 2:1 are taken into consideration. It is thus suggested that the reason why the medium becomes acidic is that the decrease in C_T is overweighed by the decrease in alkalinity. As a result, the concentration of CO_2 increases (Zeebe and Wolf-Gladrow, 2009).

1.3.6 Water masses and the oceanic fronts

Water masses and ocean fronts will be identified to help understand the carbonate characteristics. Oceanic fronts are comparatively narrow zones separating broader areas with different stratification types (vertical structure); they are accompanied by enhanced horizontal gradients of biological, chemical and physical properties (Belkin and Cornillon, 2003). Various properties characterize different depths and regions since seawater properties are not distributed uniformly. A common formation history is often shared by bodies of water that have similar properties, these are referred to as water masses (Liu and Tanhua, 2019).

In the Southern Ocean, fronts are often defined in relation to water masses (Sokolov and Rintoul, 2002; Orsi *et al*., 1995). This is evident in Figure 5 which depicts that the cool, fresh subantarctic water and the salty, warm subtropical water are separated by the Subtropical Front (STF) which is associated with strong temperature and salinity gradients (Sokolov and Rintoul, 2002). The Antarctic Intermediate Water (AAIW) is marked by salinity minima below the Subantarctic Mode Water (SAMW) thermostad. The Upper Circumpolar Deep Water (UCDW) coincides with the temperature maximum layer below θmin winter water. $\boldsymbol{\theta}$min is temperature minimum and it is sometimes called Winter Water (Sokolov and Rintoul, 2002). The northward descent of salinity minima at the Subantarctic Front (SAF) is associated with AAIW and the shoaling of UCDW across SAF is responsible for the southward increase in salinity at greater depths. Since there is a relatively uniform temperature of UCDW, the poleward increase in density is attributed to salinity. The Polar Front Zone (PFZ) corresponds to transport maxima and the southern ACC front (SACCF) is said to be the only front in the Southern Ocean that does not separate distinct surface water masses.

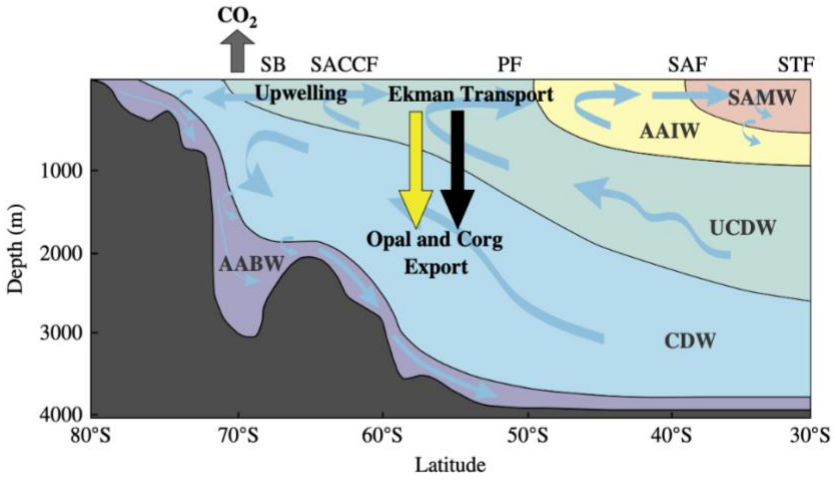

Figure 5: The illustration of Southern Ocean overturning circulation (Egan *et al.*, 2013), its relationship to the biological pump and the demonstration of how the Antarctic Circumpolar Current (ACC) drives upwelling to the south of the Polar Front (PF). Southern ACC front (SACCF); Southern Boundary (SB); Polar Front (PF); South Sub-Tropical Front (STF); Subantarctic Front (SAF); Circumpolar Deep Water (UCDW); Antarctic Intermediate Water (AAIW); Subantarctic Mode Water (SAMW) and Antarctic Bottom Water (AABW).

1.3.7 The regional contrasts in carbonate chemistry

In order to understand how the carbonate chemistry varied regionally, we will investigate how the surface gradients changed meridionally from north to south and vertically from the surface to a thousand meters.

1.3.7.1 Meridional Surface gradients

There is high natural variability in the carbonate system of polar oceans and their spatial gradients are said to be strong, this makes it difficult to differentiate between natural processes and perturbations that are a result of anthropogenic CO_2 that gradually invades the ocean (Stark *et al.*, 2018). It has been highlighted that the regional differences in biology, chemistry and circulation result in a significant heterogeneity in the spatial and temporal patterns of response (Bushinsky, Takeshita and Williams, 2019). The regional variation of carbonate parameters occurs regardless of the fact that the average pH of surface waters remains approximately 8.2 globally (Coughlan, 2013). The buffering capacity, pH and the saturation states of calcium carbonate minerals are naturally lower in oceans found in high latitudes. This is due to their cold waters which have higher solubility of CO_2 and it is anticipated that they will be the first ones to experience calcium carbonate minerals' undersaturation (Tynan *et al.*, 2016).

In fact, it is predicted that the Southern Ocean will be one of the first regions to undergo widespread undersaturation (Stark *et al.*, 2018). The onset of future ocean acidification and aragonite can be hastened by the natural seasonal variations of carbonate and pH and the results from the study of McNeil and Matear, 2008 have shown variations in the seasonal amplitude of carbonate and pH where some regions in the Southern Ocean undergo annual variability of up to 0.06 for pH and 35 mol/kg for carbonate. It is this level of natural seasonal variability in the Southern Ocean that has large implications for the onset of future ocean acidifications (McNeil and Matear, 2008). The reason why the Southern Ocean will be one of the first regions to experience undersaturation is because of the Revelle factor being high due to upwelling of waters with higher C_T / AT ratio. This higher Revelle factor reflects decreased buffering capacity which means the resistance of changes in seawater pCO_2 to changes in DIC has decreased (Williams *et al.*, 2018). This study will investigate changes in both the polar as well as the northward regions of the Southern Ocean. The pH is expected to drop by more than 0.2 units in some parts of the high latitude ocean (Cao and Caldeira, 2008) and these cold polar waters had a saturation state of about 1.4 in pre-industrial times. This makes them prone to undersaturation as the atmospheric CO_2 concentrations continue to increase. By the year 2050, it is anticipated that the Southern Ocean south of 60°S will begin to experience undersaturation if surface ocean CO_2 is assumed to be at equilibrium with the atmosphere (McNeil and Matear, 2008).

The temperature-dependent solubility of CO_2, upwelling and primary production drive horizontal distribution of C_T and CO_2. Although generally, the solubility is enhanced in high latitudes (low temperature) while less CO_2 is being absorbed in low latitudes (warm temperature), these general patterns may indicate significant deviations as a result of changes in upwelling, salinity, and biological activity (Zeebe and Wolf-Gladrow, 2009). The change in pH increases as you move southwards, causing the system to shift from being temperature dominated to being biologically dominated (Williams *et al.*, 2018).

1.3.7.2 Vertical Profiles and Sections

Biological processes have a great impact on variations in the saturation state, pH and C_T (Tynan *et al.*, 2016). In fact, the dominant regions of net CO_2 uptake are said to be determined by both surface gradients in C_T and local biological processes (Williams *et al.*, 2018). On the other hand, the Ekman convergence of C_T and the upwelling of waters high in C_T determine the locations of net outgassing of CO_2. The deep waters of the Southern Ocean are carbonate-poor but rich in C_T, the carbonate ion concentrations decline considerably when these waters are brought up into the

surface layer by upwelling.The efficiency to ventilate deep waters is also remarkable in the Southern Ocean (González-Dávila *et al*., 2011). The C_T is vertically distributed by the physical carbon pumps and the biological pumps in the ocean. The temperature-dependent differences in the solubility of CO_2 drive the physical carbon pump whereas the biomass that can be fed into the marine food webs is built up by phytoplankton using CO_2 in biologically mediated carbon pumping (Rokitta, 2012). When some of the formed biomass forms aggregates with other organic matter like marine snow and detritus, these aggregates are exported from the upper ocean as they sink to depth. The vertical depth gradients of C_T are established by the consumption of C_T in the photic zone and remineralization of exported carbon in the ocean interior while the vertical gradients of alkalinity are maintained by surface calcification and the export and dissolution of particulate inorganic carbon at depth (Rokitta, 2012).

The C_T is reduced in the surface ocean and increased in deep water (Figure 6a) due to its export to deeper layers, $CaCO_3$ production, remineralization and the organic matter taking up the carbon (Zeebe and Wolf-Gladrow, 2009).

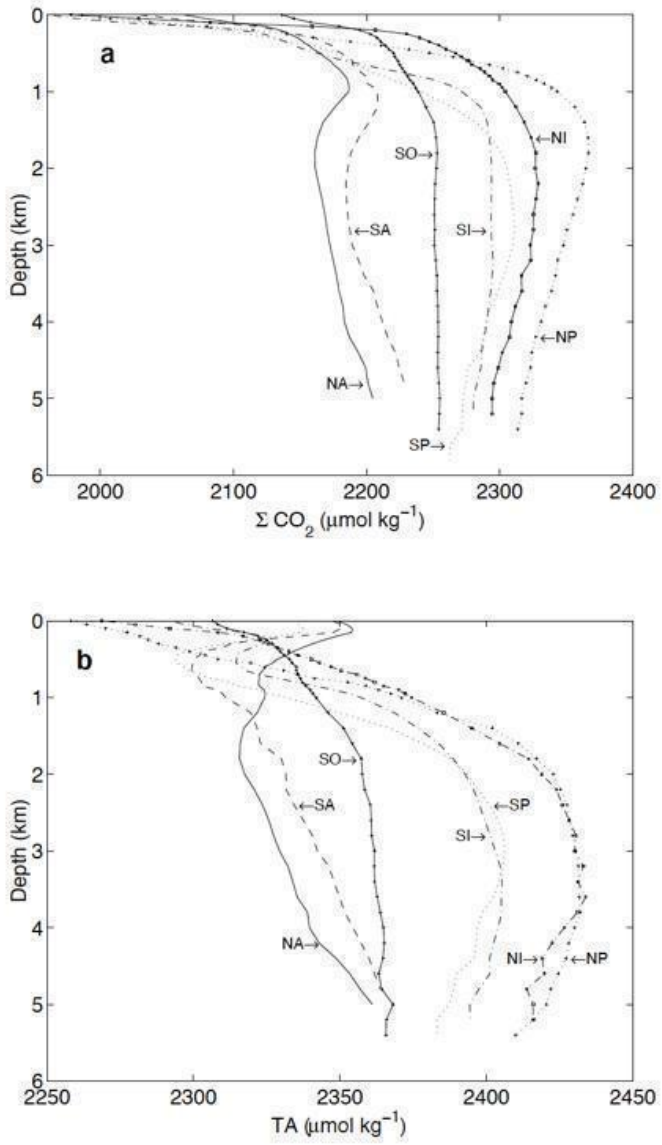

Figure 6: The $\sum CO_2$ and A_T over depth (Zeebe and Wolf-Gladrow, 2009) shown in (a) and (b) respectively. These plots show how these two parameters are vertically distributed in various oceans, where SO is the Southern Ocean.

The production and dissolution of $CaCO_3$ control the vertical profiles in Figure 6b. The uptake of carbonate ions and calcium ions reduces the A_T in the surface while the release of these ions lead to an increase in A_T. The A_T is maximum in deep water because $CaCO_3$ is re-dissolved mainly at greater depth (Zeebe and Wolf-Gladrow, 2009).

1.3.8 Seasonal changes

C_T decreases in spring-summer due to drawdown from primary production and the addition of freshwater from melting ice in the southernmost zones and due to warmer waters (Williams et al., 2018; Legge *et al.*, 2017). C_T then increases in autumn-winter due to respiration at the surface, colder waters and entrainment of higher C_T, A_T and NO_3 waters from below as the mixed layer deepens (Williams et al., 2018). Mixing with deeper waters in winter increases the C_T concentration at the surface whereas stratification may indirectly reduce C_T in spring and summer (Legge *et al.*, 2017).

The entrainment of C_T-rich waters is the most dominant driver in winter as compared to biological processes or solubility. On the other hand, shallow mixed layers evolve in summer and the C_T gets depleted by biological production, thus enriching concentrations of carbonate ions (Conrad and Lovenduski, 2015). The export production is high in summer and it is relatively low in winter, the surface C_T is thus expected to decrease in summer and increase in winter (Conrad and Lovenduski, 2015). Seasonal variability might also accelerate the onset of undersaturation with respect to aragonite (McNeil and Matear, 2008). In areas with low biological activity, sea ice-melt was found to be the key driver for the carbonate system. When primary production is intense during summer months, the calcium carbonate saturation states become typically higher, thus resulting in favorable saturation state and pH conditions for marine organisms in summer (Stark *et al.*, 2018).

However, marine organisms will be exposed to extremes in carbonate chemistry under future atmospheric CO_2 scenarios (Stark *et al.*, 2018). The pH perturbations performed in winter are thus necessary to fully represent these extremes. Undersaturation with respect to aragonite is likely to occur in winter due to enhancement of CO_2 uptake when surface temperatures are low and when the flux of inorganic carbon is enhanced by strong westerlies (Conrad and Lovenduski, 2015). The removal and addition of freshwater also affects both the A_T and C_T (Williams *et al.*, 2018).

There is a presumption that even though long-term intensifications have been observed in the open oceans, these are not the only regions where OA has been in progress. Rather, coastal zones may also be susceptible to OA due to mixing with waters from offshore open zones and through air-sea

CO_2 exchange (Ishii *et al*., 2011). It is hypothesized that polar regions will acidify more when compared to the open ocean (McNeil and Matear, 2008), especially during the winter period.

1.4 Aims and objectives

1.4.1 The aim

This study aims to characterize the seasonal meridional gradients and explain the mechanisms that may be responsible for seasonal differences of the carbonate system at the surface and upper 1000m of the water column in the Southeast Atlantic sector of the Southern Ocean.

1.4.2 Objectives

a) To observe the physics (t, S) and carbonate (A_T, C_T, pH and Ω_{Ar}) seasonal characteristics in the surface and upper 1000m of the South East Atlantic through the SCALE 2019 Winter and Spring cruises.
b) To do comparative analyses of the seasonal meridional gradients and processes that shape these gradients will be explored in the surface layer.
c) To do comparative analyses of the seasonal meridional gradients and processes that shape these gradients will be explored in the upper 1000m of the water column.

2. Methodology

2.1 Sampling stations

The winter cruise began on the 18th of July 2019 and the spring cruise started on the 12th of October 2019. The Agulhas ii research vessel departed from Cape Town and while sailing towards the Sub-Antarctic Zone (SAZ) and Polar Upwelling Zone (PUZ), we started the collection of samples from the underway surface seawater supply. The Niskin CTD casts were also deployed in successive SAZ stations (Figure 7) up to the last open ocean station in the southward leg; they were deployed to a maximum of 1000m. The ship then sailed to the Marginal Ice Zone (MIZ). Niskin CTD casts were deployed on the MIZ stations in this ice leg These deployments went to a maximum of 500m. The vessel then exited MIZ and entered the whale survey (WS) leg (57.5S, 24.0E) where CTDs were deployed to a maximum of 1000m, the final leg was towards the north along the Good Hope transect with 12 GT stations. A total of 458 CTD samples and 71 underway samples were collected in the spring cruise. Collection of underway samples was done every four hours. The winter cruise ended on the 12th August 2019 while the spring cruise ended on the 19th of November 2019. Ethical clearance was not required for this study.

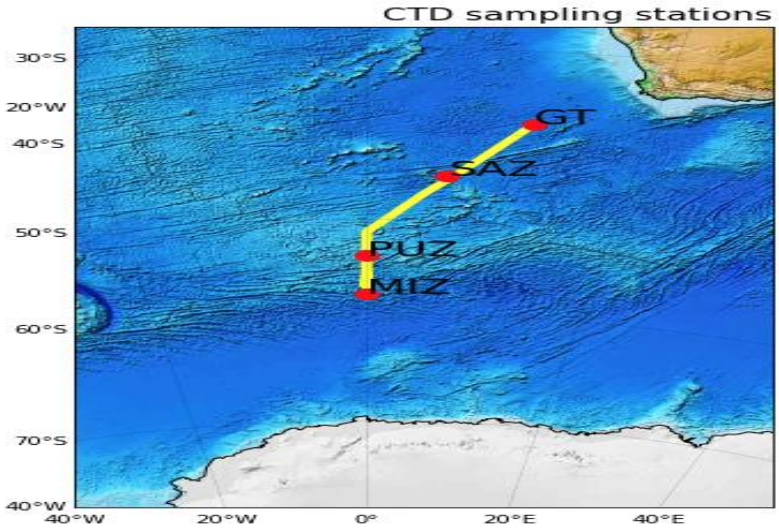

Figure 7: The course taken on the 2019 SCALE winter and spring cruise showing the main CTD sampling stations that were common between the two cruises.

2.2 Sample collection from CTDs

The CTD samples were collected immediately after the collection of oxygen samples (which have faster exchange rates) to ensure that the exchange of CO_2 with the air space was minimized.

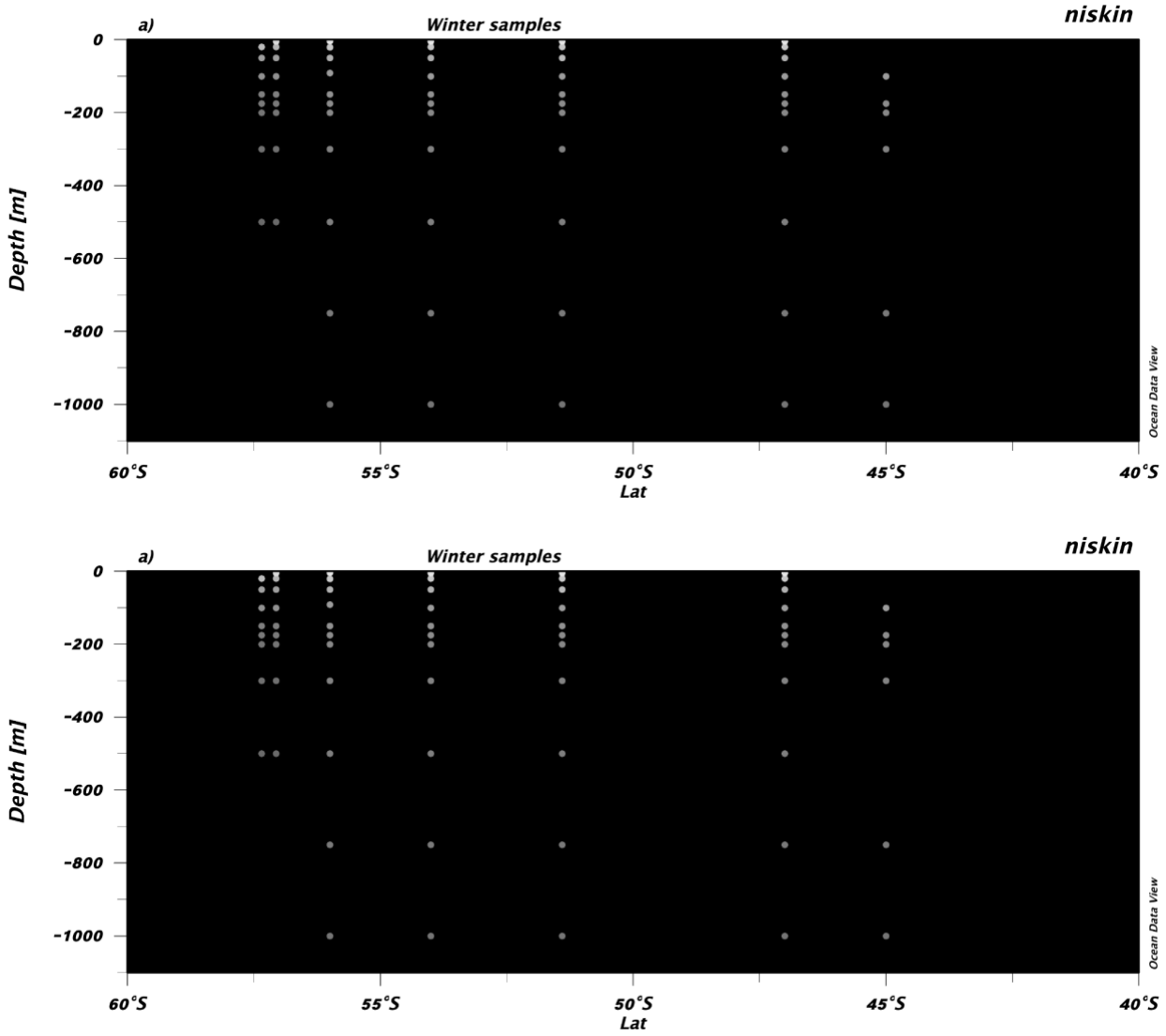

Figure 8: Shows the location and depths where CTD samples were collected in a) winter and b) spring.

To minimize bubble formation when drawing a sample, a drawing tube was used which extended from the Niskin drain to the bottom of the sampling bottle. The borosilicate glass bottles of 500ml were used as sample containers, they were rinsed and filled smoothly. The water was overfilled by the bottle volume to make sure that there was no gas trapped in the sample. These samples were taken from 12 to 13 Niskin bottles in the south leg and 24 Niskin bottles were used in the north leg. Samples were collected from five more stations in spring than in the winter cruise (Figure 8).

A headspace of 1% (Jones *et al.,* 2016) of the bottle was adjusted to allow water to expand in higher temperatures. This space was small enough to make sure that the amount of gas exchange between the headspace and the entire sample was minimized. Greased glass stoppers were used to seal all samples and rubber bands were used to hold them in place. Both the underway and CTD samples were poisoned with 120µl of mercuric chloride to minimize biological activity which might alter carbon distributions in the samples. The samples were analyzed within 12 hours or kept at room temperature in the dark.

2.3 Measuring A_T and C_T

Most of the carbonate species cannot be measured directly. From the four parameters of the carbonate chemistry that can be determined analytically: pCO_2, pH, A_T and C_T; only two are required along with temperature, pressure and salinity measurements for the carbonate system to be fully characterized. Here, we only measured A_T and C_T using the VINDTA system.

2.3.1 A_T analysis

For A_T analysis, a known amount of each sample was dispensed into a cell where it was titrated with about 20 increments of hydrochloric acid. During this potentiometric titration, the 0.25M HCl was added until all proton acceptors (weak bases) had reacted. The added HCl contained sodium chloride (0.25M in NaCl) that adjusted ionic strength so it would be approximately the same as that of sea water. Manual dosing of the acid was done using a titrino to remove bubbles from the tubes prior to dispensing the required amount of acid. This titration worked out the amount of acid needed for titration of all of those species and the endpoint was reached when the pH was about 4.3. At this pH, the hydrogen ions are equal to bicarbonate ions and both the bicarbonate and carbonate ions have been converted to carbonic acid. Both the electromotive force (e.m.f) of the pH cell as well as the total volume of acid added were recorded by the computer using a full titration curve known as the Gran plot was used for analysis (Murray, 2004). The addition of acid changed the pH, so temperature was controlled throughout the analysis. The circulating water bath was used to maintain it at 25˚C using VINDTA.

2.3.1.1 Parameterization of A_T

Parameterization of A_T was considered to calculate the A_T in both profiles and underway analysis using the LIAR method for winter and spring because the winter data were not reliable. Precipitation and sea-ice melting (freshwater addition) and change in salinity due to removal of freshwater (sea-ice formation and evaporation) are the main drivers of A_T variability in the surface ocean (Lee *et al.*, 2006). Surface A_T concentrations are also increased by the progressive increase in convective mixing of A_T-rich deep waters at higher latitudes (south of 30˚S) during seasonal cooling. Therefore, there is a negative correlation between sea surface temperature (SST) and A_T. The SST is the primary criterion for selecting an appropriate algorithm for predicting A_T from SST and SSS (Lee *et al.*, 2006). The A_T was derived from the SST and SSS using the following equations:

$$A_T\_pred = (2305) + (52.48) * (SSS - 35) + (2.85) * (SSS - 35)^2 - (0.49) * (SST - 20) + (0.086) * (SST - 20)^2 \quad (7)$$

$$A_T\_pred = \propto_0 + \propto_S S + \propto_\theta \theta \quad \text{where S is salinity and } \theta \text{ is potential temperature} \quad (8)$$

Equation 7 relates surface A_T to SST and SSS where a geographic boundary is between south of 30˚S and 70˚S, for SST that is less than 20˚C and SSS from 33 to 36 (Lee *et al.*, 2006). The Locally Interpolated Alkalinity Regression (LIAR) method with equation 8 (Carter *et al.*, 2016) was also used. The A_T in both profiles and underway analysis were calculated using the LIAR method for winter and spring because the winter data were bad. Firstly, the regression coefficients were interpolated and the second step was to use those coefficients to calculate the A_T estimates directly from equation 8.

2.3.2 C_T analysis

The VINDTA system was used for C_T analysis. The coulometric cell was washed and dried in the oven at 50˚C overnight before use; this was done to ensure that the frit separating the anode and cathode chambers was completely dry and the build-up of organic films was also prevented. This frit allowed a flow of electrons. The cap and electrodes of the coulometric cell were cleaned using acetone and then rinsed with deionized water. The cell had a cathode solution of 100ml on the bigger chamber and an anode solution 1cm lower than the cathode solution level on the smaller

chamber. Potassium iodide crystals were added to the anode chamber prior to adding the anode solution. This was done to ensure that the anode solution (potassium iodide in water) remained saturated.

Once the coulometric cell was prepared and the setup was done in the coulometer, about 30ml of each sample was dispensed from the sampling bottle into a stripping chamber where it was acidified by 5ml of phosphoric acid (6%). The bicarbonate and carbonate were converted to unionized carbon dioxide and moisture from the sample was trapped by the Peltier. In order to extract the CO_2 that would then be measured, the gas stream was purged with nitrogen which acts as an inert carrier gas (CO_2-free) and it was then absorbed in the coulometric cell by a solution containing ethanol (ethanolamine). This reaction formed a weak acid. Hydroxide was produced electrolytically in the cathode chamber of the coulometric cell and it was used as a strong base to titrate that acid. The amount of OH^- that had to be generated to reach the original pH was thus measured and it is proportional to the amount of CO_2 (Murray, 2004). At the end of the titration the solution in the coulometric cell turned blue when the endpoint was reached. Thymolphthalein was used as an indicator. The data from the coulometer was recorded on a spreadsheet by the computer after an integration of successive coulometer readings.

2.4 Quality assurance of measurements

In order to obtain stable measurements, the facilities and the equipment used were properly maintained. Good laboratory practices were followed. The titration cell was wiped thoroughly before placing it in the coulometer and nitrile powder-free gloves were used to make sure there were no fingerprints that would interfere with transmittance. To minimize any unwanted bias results, good measurement practices were also followed. The well-written standard operating procedures from Andrew Dickson were also adopted. Dickson's Certified Reference Material (CRM) samples were used to determine the accuracy of the VINDTA machine before and after running about 20 samples. The batch numbers for CRMs that were used as controls are 159 and 183. A factor derived from the theoretical and the measured values of these CRMs was used for correcting the measured A_T and C_T values. The theoretical values were measured with high accuracy by A. Dickson (Zeebe and Wolf-Gladrow, 2009). Test samples that were also analyzed prior to running our actual samples. To check the precision, eight samples were collected from the same Niskin bottle that was closed at 10-meter depth in winter. From the spring cruise, precision

was determined using replication of ten samples from the same CTD Niskin bottle. These were then used to calculate the standard deviations of C_T and A_T.

The accuracy of both the measured (input) parameters and the thermodynamic constants determines the accuracy of the derived values while the imprecision of measured values limits the precision of derived values (Clayton *et al.*, 1995). The pH and Ω_{Ar} were derived using A_T and C_T. So, we assessed the sensitivity of pH and Ω_{Ar} to changing C_T and A_T content since calculations of the parameters depend less on the choice of constants and more strongly on the choice of input pair of carbonate system variables (Raimondi *et al.*, 2019). Transformation of CO_2 into carbonate species as well as the solubility of CO_2 are governed by the equilibrium constants (K_0, K_1 and K_2), so the internal consistency is also affected by how well these dissociation constants describe the carbonate system equilibria (Raimondi *et al.*, 2019).

2.5 Carbonate system calculations

The CO_2SYS computer program (available as Excel macros) was used to calculate the concentrations of other unknown concentrations of carbonate species: the pH as well as the saturation state of calcite and aragonite. The equilibrium constants were used together with the two measured parameters (C_T and A_T) for these calculations. The temperature, pressure, salinity and nutrients were also included for the input data. The salinity and temperature measurements helped in determining the equilibrium constants. Since calcium ion concentration is also required when estimating the saturation state, salinity values were also used for its estimation. The atmospheric pressure of 1 atm was used because it is considered to be equal to the total pressure in CO_2SYS (Raimondi *et al.*, 2019). After enabling macros, the recommended constants and pH scale were selected. These are the total pH scale, Mehrbach *et al.* 1973 constants and the Dickson $KHSO_4$ constant (Zeebe and Wolf-Gladrow, 2009). It is noteworthy that the choice of equilibrium constants is constrained by the choice of pH scale.

3. Results

3.1.1 The Surface Seasonal Physical Characteristics

Here we characterize the seasonal oceanographic context using surface underway observations of Sea Surface Temperature (SST) and Sea Surface Salinity (SSS) (Figures 10a and 10b) from both Winter (July-August 2019) (40˚S - 56˚S) and Spring (Oct - Nov 2019) (40˚S - 57˚S). Since the ocean fronts are important in understanding salt and heat transport (Belkin and Cornillon, 2003), this section also identified the frontal zones at the surface by means of SST and SSS (Figure A1). The characteristics defining fronts are shown in Table 1.

Table 1: The ocean fronts, observed changes in Sea Surface Salinity (SSS), Sea Surface Temperature (SST) and the locations of frontal zones in winter and spring (see also Figures 5, 7, 9, 10).

Ocean front range	Change in SSS	Change in SST (˚C)	Frontal position
South Sub-Tropical Front (STF) to Subantarctic Front (SAF)	Decrease from 35.25 to 33.57 in winter and from 34.5 to 34.25 in spring.	Decrease from 15 to 7.3 in winter and from 12.5 to 8.5 in spring	At 40.83˚S in winter and 40.57˚S in spring
SAF to Polar Front Zone (PFZ)	Decrease from 33.57 to 33.51 in winter and from 34.25 to 33.51 in spring	Decrease from 7.3 to 4 in winter and from 8.5 to 4 in spring	Around 44.21˚S in winter and 44.68˚S in spring
PFZ to Southern ACC front (SACCF)	Weak gradient in both seasons. Increasing from 33.51 to 33.7 in winter and from 33.51 to 33.6 in	Sharp decrease in both seasons. Decreasing from 4 to 1 in winter and from 4 to 1.5 in spring.	Around 48.87˚S in winter and 48.92˚S in spring

	spring.		
SACCF to Southern Boundary of ACC (SBdy)	Increase from 33.7 to 33.8 in winter and 33.6 to 33.7 in spring.	Decrease from 1 to -2 In winter and from from 1.5 to 1 in spring.	At 52.13˚S in winter and 52.65˚ S in spring
SBdy to 57˚S	Increase from 33.8 to 33.81 in winter and decreased from 33.7 to 33.52 in spring	Increase from -2 to -1 in winter and from 1 to 2 in spring.	Around 55.95˚S in winter and 56.21 in spring

Three dominant water masses were identified from the surface observations in both winter and spring (ESACW, AASW and AAIW) (Figure 9). The seasonal T-S plots with the surface observations are depicted in Figure (9). The Eastern South Atlantic Central Water (ESACW) is warmer (7.5˚C to about 15˚C), saltier (between 34 and 35.5) but less dense (26-26.5 kg/m^3) than Antarctic Surface Water (AASW) (<0˚C; 33.66-33.78; 27-27.25 kg/m^3) and Antarctic Intermediate Water (AAIW) (2-6˚C; 33.57-33.72, 26.25-27 kg/m^3). Surface ESACW is generally warmer and saltier in spring (about 8-12.6˚C; 34.2-34.6) than winter (about 7.5-11˚C;34.1-34.2) except for one point where winter is warmer and saltier (15.2˚C; 35.2). The AAIW is about 0.45˚C warmer in spring than in winter while AASW is about 1˚C colder in winter than in spring.

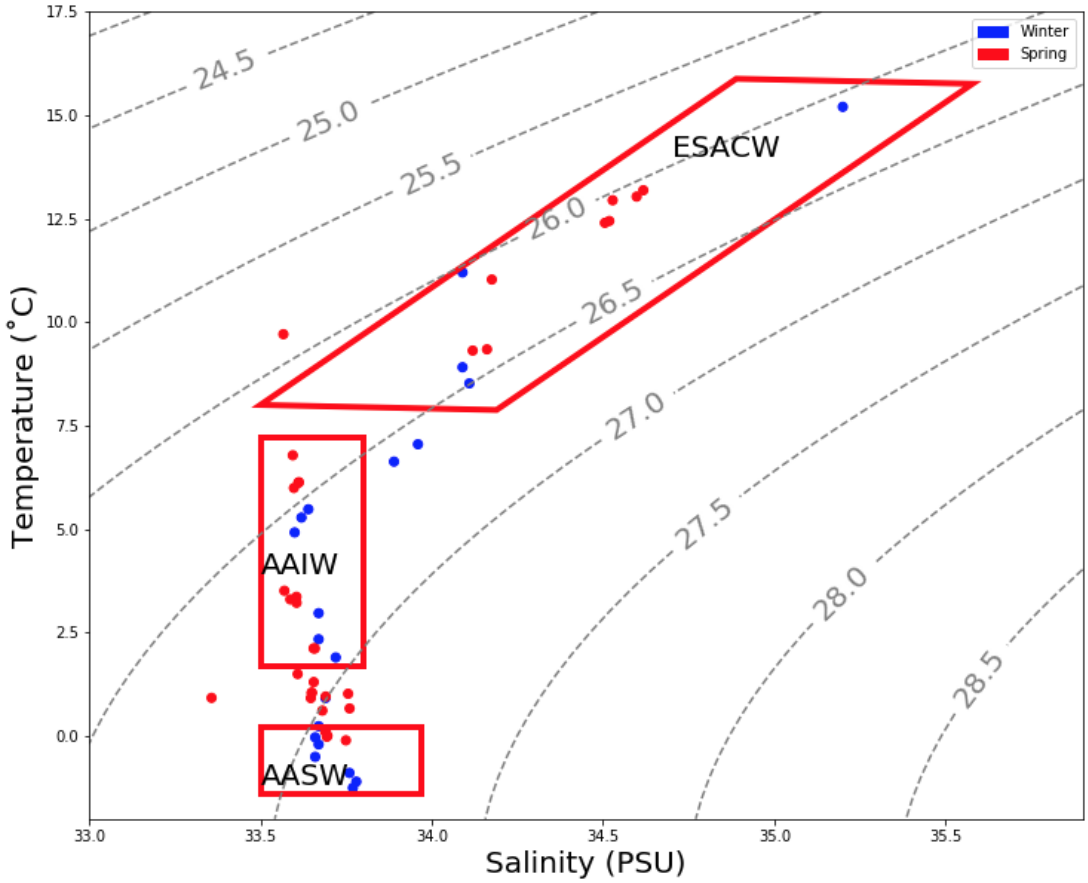

Figure 9: The T-S diagrams of underway samples collected in winter and spring showing water masses that were characterized from surface temperature (˚C) and salinity. Water masses with similar properties are marked by the red boxes and the isopycnals show potential density (sigma-theta). Their T-S ranges are 7.5-15˚C, 34.3-35.4 for ESACW; 2-6˚C, <34.4 for AAIW and the AASW is < 0˚C but may rise to 2.5˚C near PFZ (Carter, McCave and Williams, 2008), with SSS that is < 34.

The surface - underway observations of SST and SSS show the expected temperature and salinity gradients (Figure 10) with warmest SST (> 10˚C) north of the SAF in the STZ near 40˚S and lowest (<2˚C) near 60˚S in both seasons. Our data shows that SST is consistently warmer by 0.2 - 2˚C in the spring south of the SAF (Figure 10a). According to Figures 9 and 10, the ESACW is found to the north of SAF (40˚S-45˚S), the AAIW is between SAF and SACCF (45˚S-52.5˚S) while AASW is in the vicinity of the SBdy (near 55˚S).

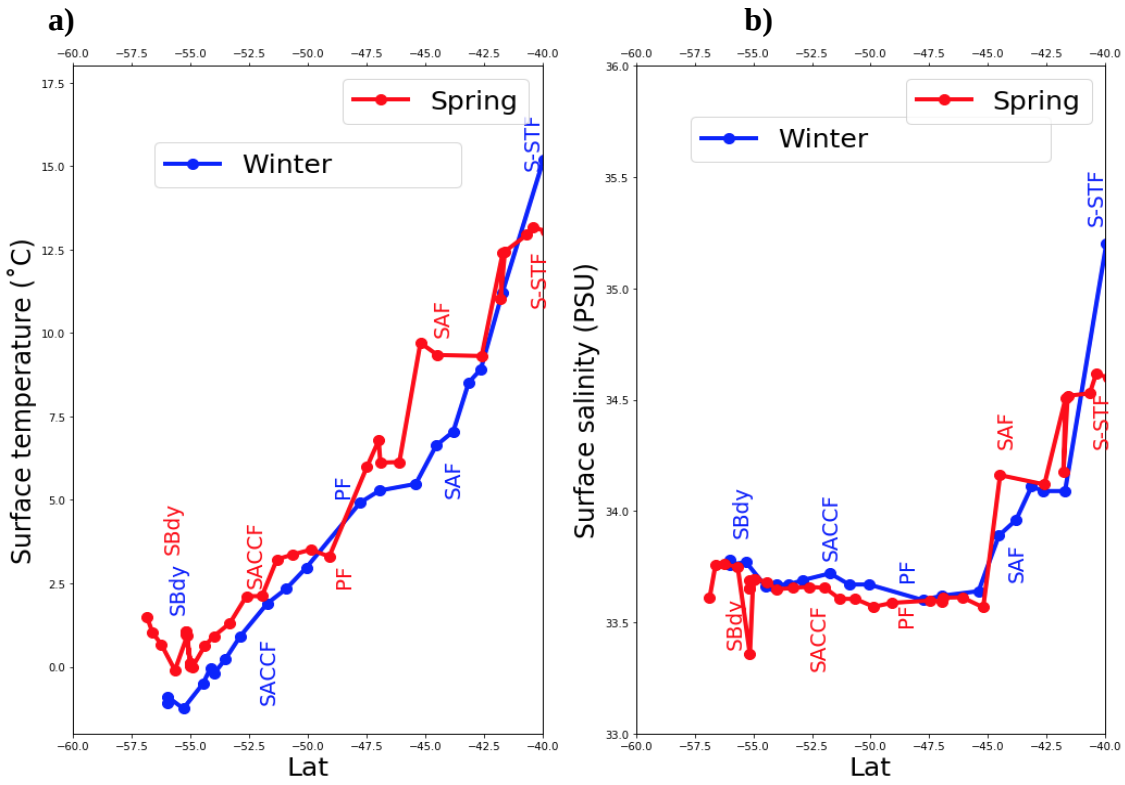

Figure 10: The a) Sea Surface Temperature and b) Sea Surface Salinity of samples collected along the ship's track. Five frontal zones were identified: the Southern Boundary of ACC (SBdy), southern ACC front (SACCF), Polar Front Zone (PFZ), Subantarctic Front (SAF) and Subtropical Front (STF) labeled in blue for winter and red for spring.

Figure (10) also revealed that the SSS meridional gradient has a minimum between the SAF and the PFZ (45˚S-49˚S) with a weak but significant increasing gradient (33.36-33.78) to the south of the PFZ (47˚S-57.5˚S) and a strong gradient (33.57-35.20) to the north of the SAF (40˚S-45˚S). It shows that south of the SAF, SSS is ±0.04 higher in winter than in spring and it is lowest near 45˚S but ±0.02 lower in spring than in winter.

3.1.2 The Surface Seasonal Carbonate Characteristics

This section provides the results to characterize the carbonate properties (C_T and A_T) for the meridional gradients in winter and spring (Figure 11 a & b). The characterization is done using the boundaries and zones defined by the SST and SSS oceanographic properties in each period (Figure 11 a & b) and Table 1. The ratio of A_T:C_T gradient is shown in Table 2 (The slope is in Figure A3). The distribution of pH and Ω_{Ar} (Figures 12) has also been provided. Our winter and spring data were compared to the work done at other times of the year like the summer data from SANAE

cruises and it was found that in summer, the general trend of C_T was a meridional increase while A_T followed the SSS trend (Figure A14). The positive anomaly in SANAE57 A_T especially south of the PF suggests that these anomalies need to be investigated.

3.1.2.1 Surface C_T and A_T

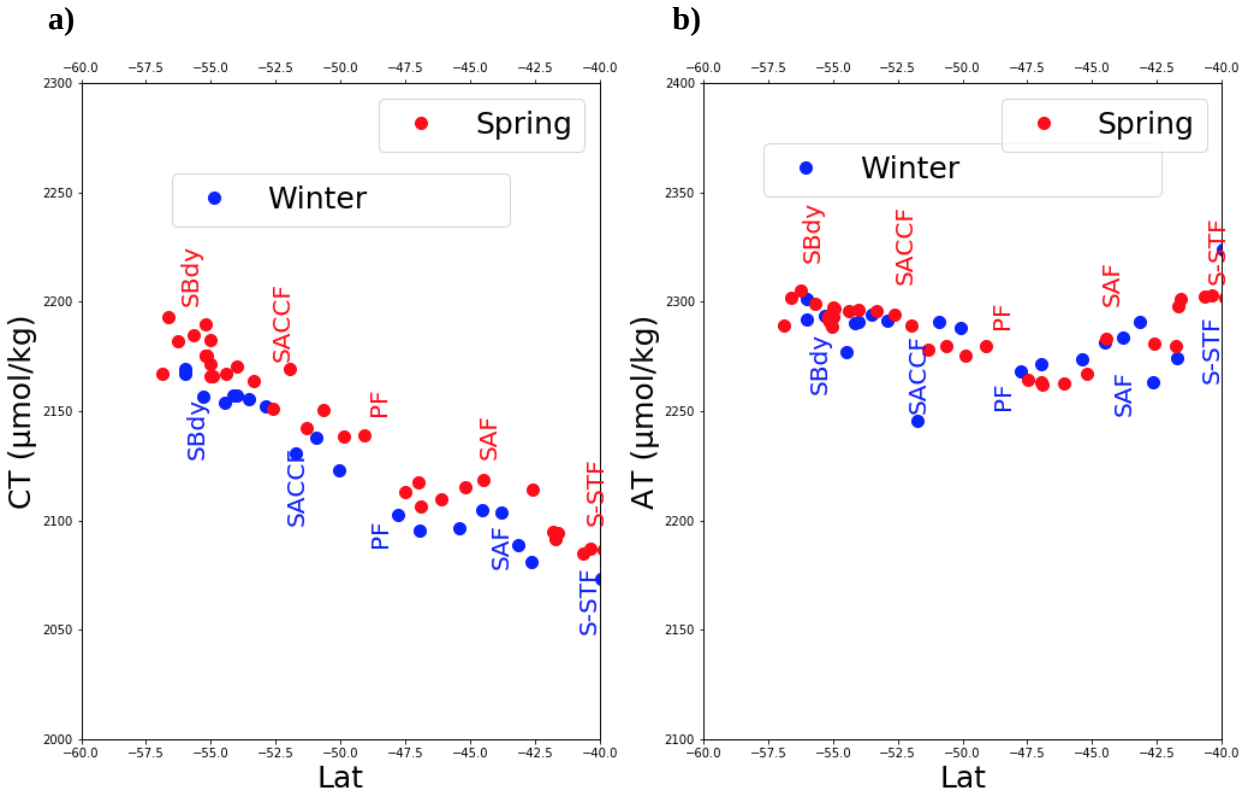

Figure 11: The surface meridional gradient of a) C_T and b) A_T with the frontal zones- Southern Boundary of ACC (SBdy), southern ACC front (SACCF), Polar Front Zone (PFZ), Subantarctic Front (SAF) and Sub-Tropical Front (STF) labeled in blue for winter and red for spring.

Figure 11 shows the distribution of C_T and A_T and the presence of the identified zonal regimes at the surface (Figure 11 a & b). Surface C_T and A_T plots (Figure A3) and Table 2 show that the surface C_T and A_T increased (by a ratio of 1:1) meridionally south of the PFZ in both seasons. In both seasons, the C_T has a consistent meridional poleward increase with a local peak from S-STF to SAF (40˚S-44˚S) where it increased by 30µmol/kg in winter and by 28µmol/kg in spring. Although the general trend was still a meridional increase, other local anomalies were observed from SAF up to north of PFZ (44˚S-47˚S) where C_T declined slightly by 8µmol/kg in winter and by 6µmol/kg in spring. From there it increased up to 2169µmol/kg in winter and 2193µmol/kg in spring from south of PFZ (49˚S) until SBdy was reached near 57˚S.

The C_T has comparable gradients but is higher in spring than winter, with the mean seasonal differences that varied across the three water masses. The AAIW had the greatest mean seasonal difference of 21µmol/kg, the AASW had a mean seasonal difference of 15µmol/kg while the least mean seasonal difference of 8µmol/kg was in the ESACW.

Table 2: The surface C_T and A_T south of 50˚S in winter and spring

	A_T average (µmol/kg)	C_T average (µmol/kg)	A_T:C_T ratio
Winter	2286.84	2150.90	1:1
Spring	2292.26	2169.10	1:1

The trend of A_T follows that of SSS and the A_T is roughly equal in both seasons. Similar to the SSS gradient, the A_T meridional gradient also has a minimum between the SAF and the PFZ (44˚S-49˚S) with a weak but significant gradient (2280-2305µmol/kg) increasing to the south of the PFZ (50˚S-57.5˚S) and a strong gradient (2302-2271µmol/kg) decreasing to the north of PFZ (40˚S-47.5˚S). For both seasons, the ratio of the slope dC_T/dA_T from 50˚S to 60˚S is 1:1 (Table2).

3.1.2.2 Underway surface pH and Ω_{Ar}

a) Surface pH **b) Surface Ω_{Ar}**

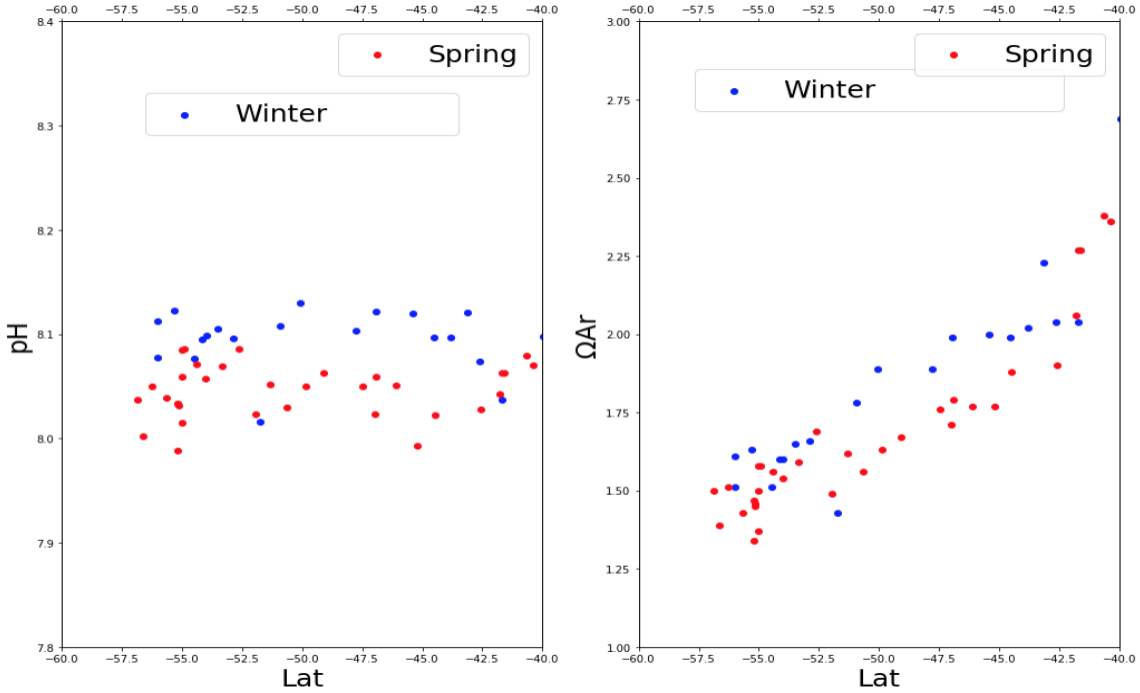

Figure 12: The surface meridional gradients of a) pH, b) Aragonite saturation states (Ω_{Ar}).

The results from underway pH and Ω_{Ar} observations (Figure12) revealed that apart from some local spatial variability, the meridional gradient of pH was close to zero although it was higher (mean of 8.10 units) in winter, ranging from 8.02-8.13 units while lower values (mean of 8.05) were found in spring (7.98-8.09 units) from 40-57˚S. In contrast, the Ω_{Ar} had a pronounced meridional gradient sharp decrease (about 2.30 to about 1.3 units) from north to south and some local variability near SBdy. Consistent with pH, Ω_{Ar} was 0.1 units higher in winter than in spring.

3.2.1. Seasonal Physical Characteristics of the Meridional Section to 1000m

The oceanographic characteristics of water masses were assigned using SST and SSS ranges from table 3. This table was constructed using characteristics taken from Emery and Meincke, (1986) and it was used to locate the water masses (Figures 13, 14 and 16). Emery, (2015); Liu and Tanhua, (2019) and Liu and Tanhua, (2021) were also used in characterizing the water masses. Winter Water (WW) is a temperature minimum layer with potential temperature ranging from -1.9 ˚C and -1.5 ˚C and salinity between 34.2 and 34.5(Tomczak and Liefrink, 2005).

Table 3: t-S characteristics of water masses from the upper 1000m in the Southeast Atlantic sector of the Southern Ocean

Layer	Depth (m)	Temperature (˚C)	Salinity	Potential Density (kg/m^3)	Water mass
Surface waters	0-500	5.0-18.0	34.3-35.8	26-27.20	ESACW
Intermediate waters	500-1500	2-6	<34.4	27-27.10 and 27.40	AAIW
Deep waters	200-1000	0.1-2.0	34.62-34.73	Higher than 27.80	CDW

Characteristics including depth, SST,SSS and potential density (sigma-theta) were used to define the water masses (Table 3). The seasonal t-S plots are also depicted for profile observations (Figure 13).

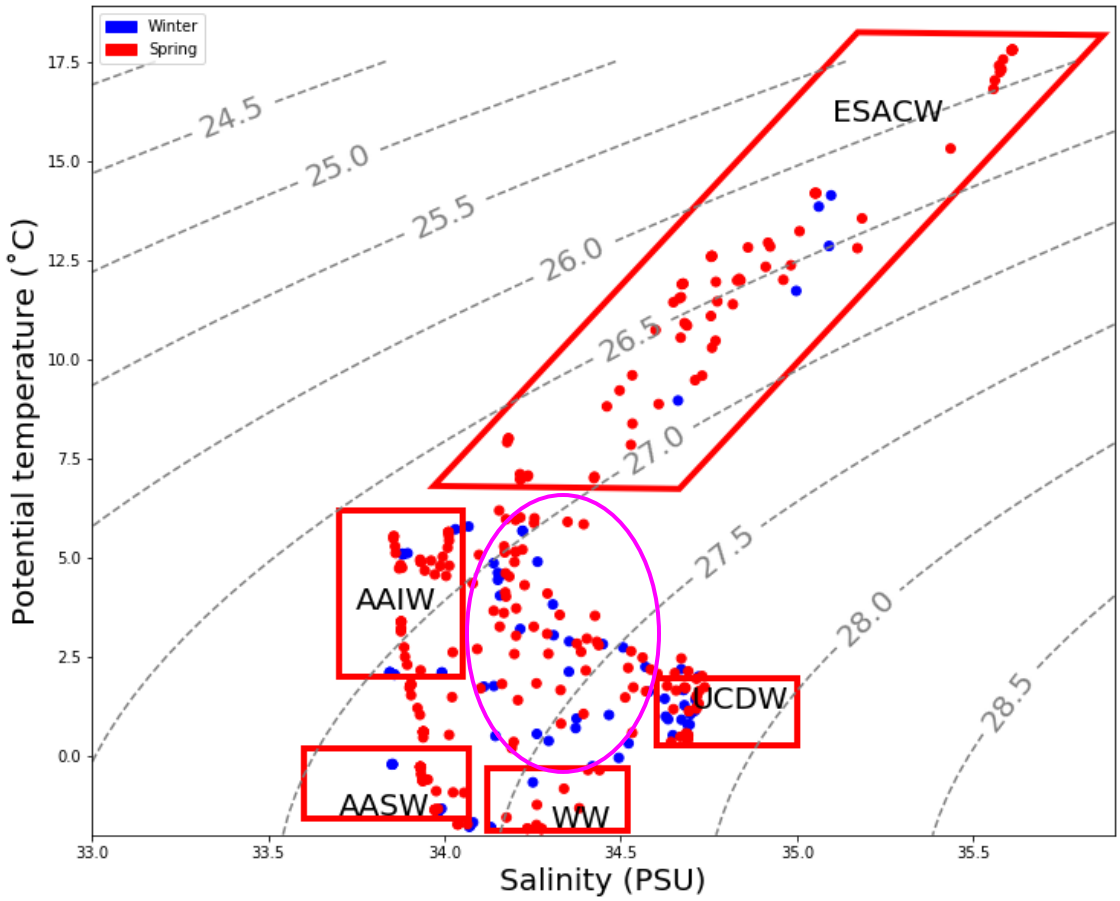

Figure 13: T-S Diagrams for the upper 1000m of the water column showing the Eastern South Atlantic Central Water (ESACW), Antarctic Intermediate Water (AAIW), Winter Water (WW), Antarctic Surface Water (AASW) and the Upper Circumpolar Deep Water (UCDW) located in winter and spring. Water masses with similar properties are marked by the red boxes and the isopycnals show potential density. The circle shows mixing of UCDW with AAIW, WW, AASW and ESACW.

Figure (13) shows that the ESACW has the largest salinity, temperature ranges and has a wide range of density anomaly (6-17.5˚C; 34-35.5; 25.75-27 kg/m^3) compared to the AAIW (2-5.5˚C; 33.84-34.00; 26.75-27.25 kg/m^3) while CDW has the low temperature (0.33-2.19˚C), high salinity values (34.47-34.74) and its density only ranges from 27.75-27.85 kg/m^3. The AASW and WW have temperatures that are below 0˚C (-1.85 to -0.05˚C) but WW is saltier and denser (34.24-34.49; 27.5-27.75 kg/m^3) than AASW (33.85-34.04; 27.25-27.5 kg/m^3). There is a linear T-S relationship in the ESACW. Figure 13 also shows that there is extensive mixing between UCDW and all four water masses (AASW, WW, AAIW and ESACW) in the upper water column in both winter and spring.

Meridional sections of temperature (˚C), salinity obtained from CTD-Rosette profiles in both winter and spring cruises are depicted in Figure (14). It shows the 5 main water masses characterized by their t and S properties.

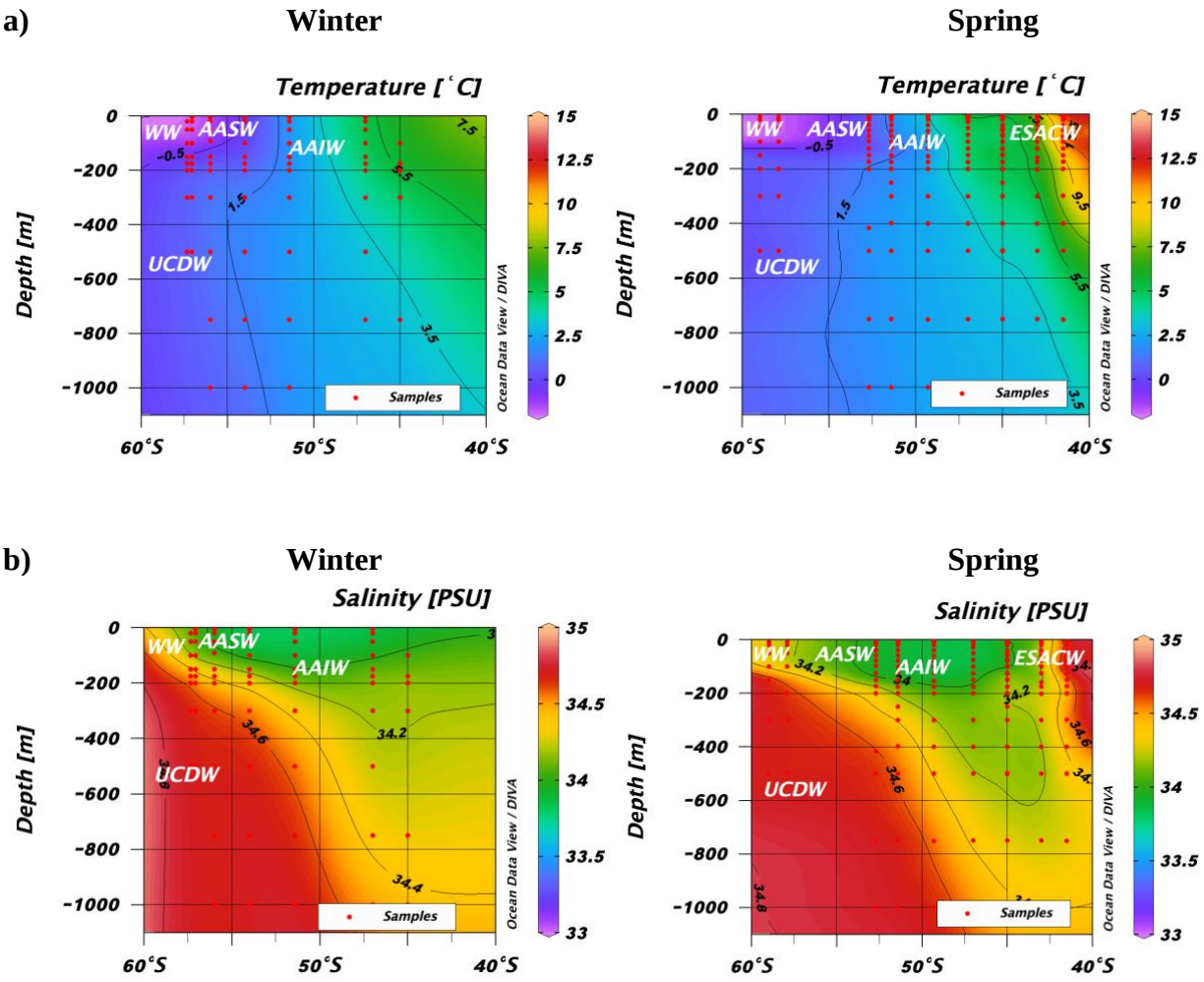

Figure 14: Vertical distribution of a) temperature (˚C) and b) salinity in winter and spring

This figure also shows meridional temperature and salinity gradients that extend down to 1000m (Figure 14 a&b). The surface is stratified (0-200m) while the water is well mixed below 200m in both seasons. Warmer waters are found at the surface near 40˚S i.e the ESACW (in spring) and there are colder waters such as the UCDW (200m-1000m) in the deeper parts of the ocean and in the upper 200m, near 60˚S i.e WW. There is a min of -0.5 near 60˚S in both seasons and a max of 7.5˚S near 40˚S at the surface in winter. In spring, the highest temperature is 11.5˚C near 40˚S at the surface. The winter and spring SSS (Figure 14b) shows upwelling of UCDW and formation of AAIW with salinity minimum (34-34.2). Subtropical high salinity (34.6) was observed at the northern boundary (40-42˚S) in spring.

Salinity increases with depth and meridionally from north to south in both seasons, ranging from about 32 at the surface, near 40˚S (except for spring where SSS is high) to about 34.8 near 60˚S at about 1000m. The AAIW sinked to about 400m in winter and it was even deeper in spring (up to 600m). The identification of possible eddies is also shown in Figure 15.

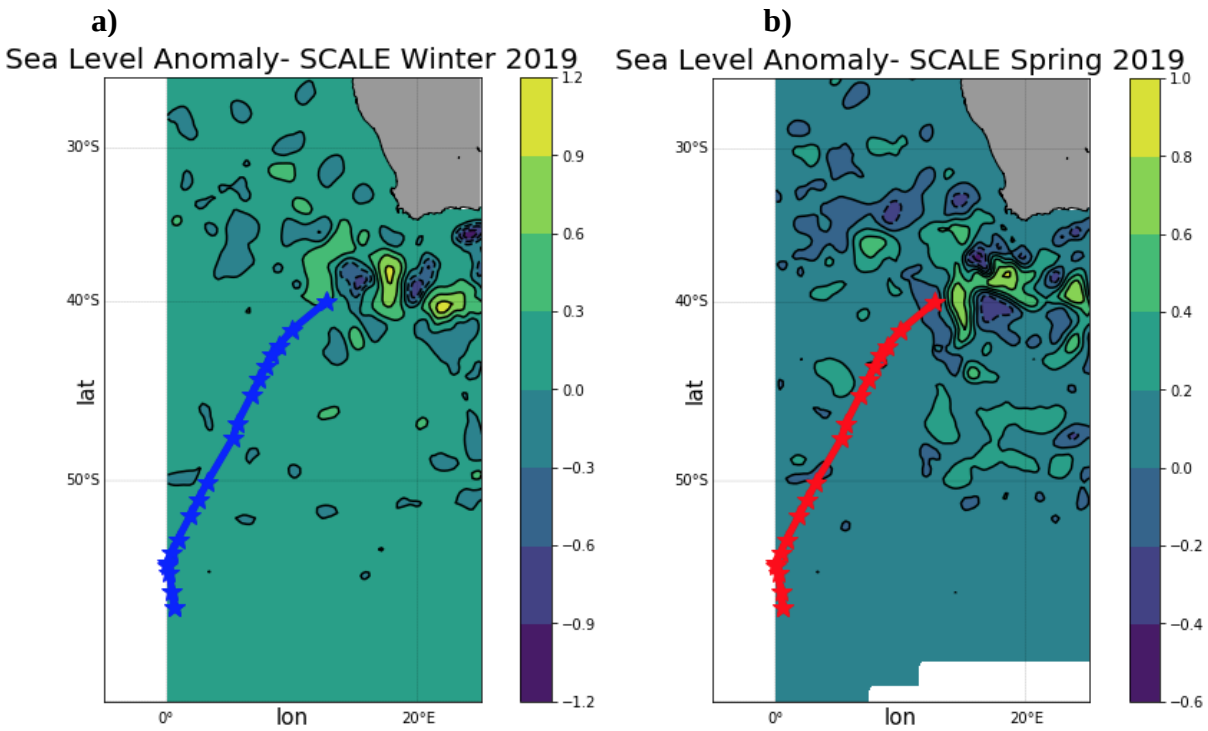

Figure 15: Showing the eddies that were detected along the GoodHope line in a) winter and b) spring. The Sea Level Anomaly (SLA) data were taken from the Copernicus site.

Anticyclonic eddies were touched at about 40-42˚S in winter. In spring, major cyclonic eddies were crossed over at about 40-42˚S and at 50˚S (Figure 15).

3.2.2 Carbonate characteristics of Seasonal Meridional Sections

The quality of winter A_T data was not reliable. It showed values as high as 2400µmol/kg (Figure 16a) so the interpolation LIARv2 method (Carter *et al.*, 2016) was used to derive the A_T values (Figure 16b). For consistency, the LIARv2 method was used for both winter and spring even though spring had good A_T data. This is evident in that the spring A_T LIARv2 results are similar to the observed A_T results. The mean difference of 0.48µmol/kg was calculated from the averages of observed A_T (2302.60µmol/kg) and calculated LIAR A_T (2303.08µmol/kg).

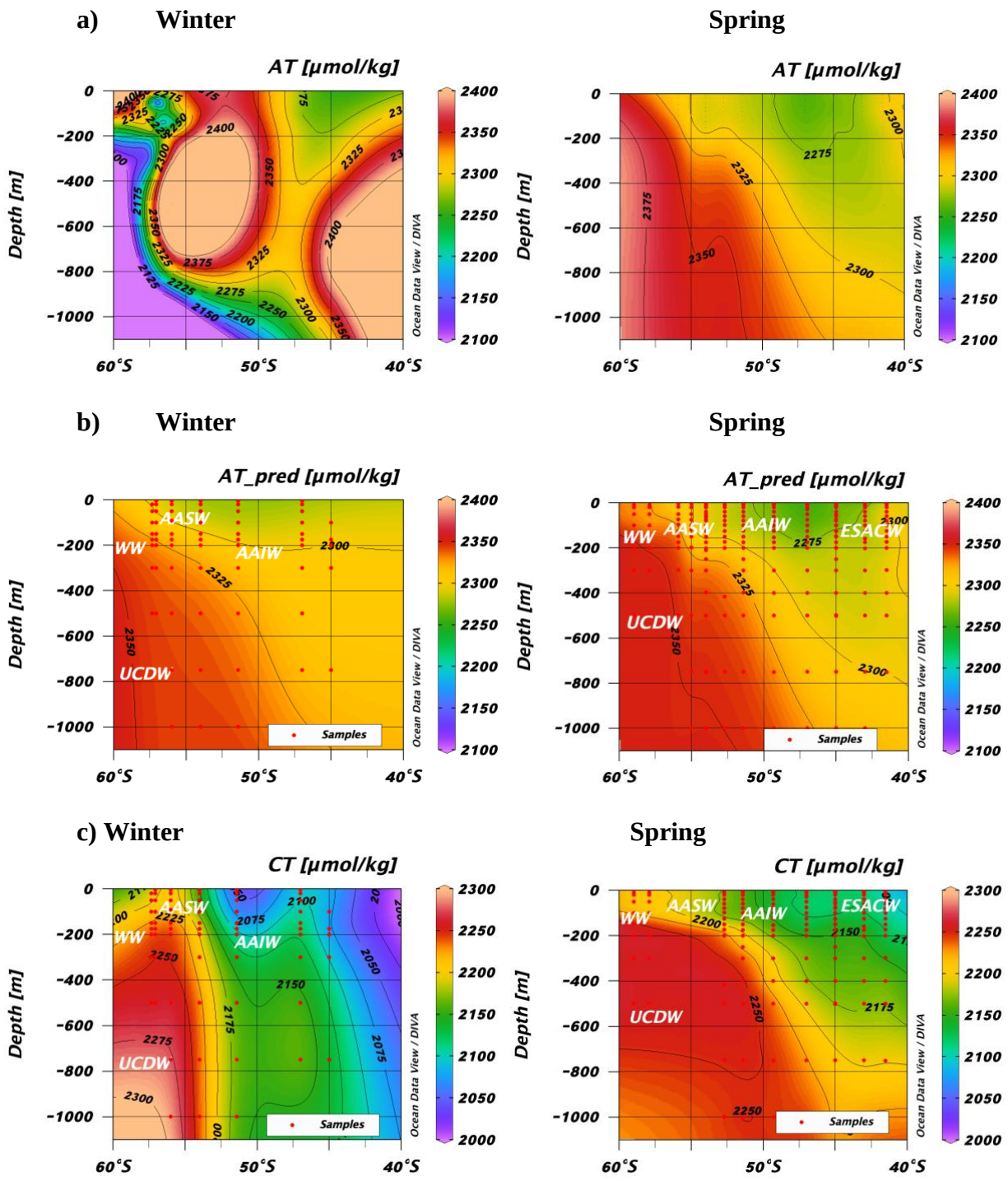

Figure 16: Vertical sections of a) The original A_T for winter and spring, b) A_T predicted from LIARv2 and c) The C_T for winter and spring. Only b and c were used for the results and discussion.

The trend of photosynthesis and respiration is similar to that of the removal and invasion of CO_2, except that the nutrients slightly change the A_T when they are being released or taken up (Zeebe and Wolf-Gladrow, 2009). Since the alkalinity is increased by biological consumption of nitrate and other species like phosphate and sulphate (Fry et al., 2015), we would expect A_T to decrease in winter when biological consumption is reduced and replaced by remineralization, which includes nitrification of the PP flux as well as the entrainment of aged CDW upwelled waters.

The vertical meridional distribution of C_T and A_T (Figure 16) shows that the UCDW had the highest C_T and A_T values in both seasons. The A_T of UCDW is just over 2300µmol/kg in both seasons but the C_T in UCDW is higher in winter (max of 2295.68µmol/kg) than in spring (max of 2262.61µmol/kg). The highest C_T in winter is further south (south of 55˚S) and further down (below 800m) while C_T is uniformly distributed south of 45˚S and below 200m in spring. The lowest A_T values were observed in the AAIW and they are 2279.55µmol/kg and 2255.42µmol/kg in winter and spring respectively. The AAIW sinks deeper in winter (Up to 1000m) than in spring (up to 600m). The meridional gradient of C_T is stronger in winter (2005.91µmol/kg near 40˚S to 2295.68µmol/kg near 60˚S) than in spring (2057.99µmol/kg near 40˚S and 2262.61µmol/kg near 60˚S). The ESACW is was present only in spring. In the region where we identified ESACW in spring, winter had a relatively low C_T of just 2005µmol/kg.

3.2.3 Seasonal pH and Ω_{Ar} Sections

This section describes the differences in pH and Ω_{Ar} meridional sections between winter and spring. The pH and Ω_{Ar} were calculated from LIARv2 A_T for both periods. The sections show the vertical distribution of pH (Figure 17a) and Aragonite saturation state (Figure 17b).

3.2.3.1 pH and Ω_{Ar} Sections

a) Winter **Spring**

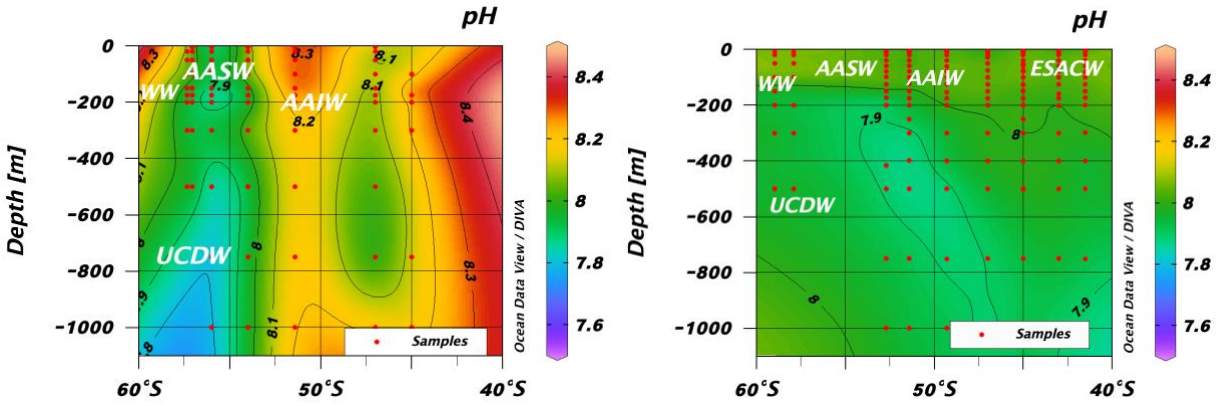

b) Winter **Spring**

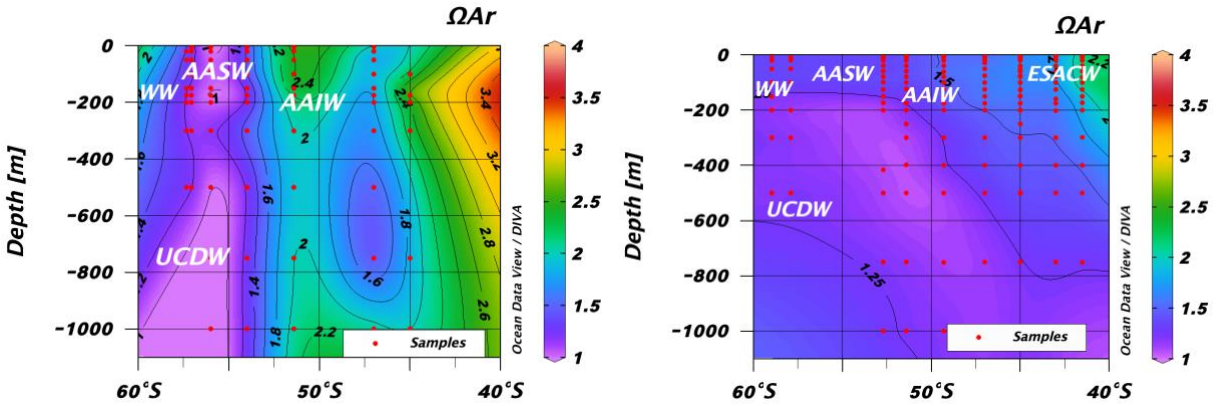

Figure 17: Vertical sections of a) pH, b) aragonite saturation state for winter and spring. The A_T values used to derive pH and Ω_{Ar} were predicted using the LIARv2 method.

The pH and Ω_{Ar} gradients are stronger in winter than in spring. The weak spring gradients reflect the uniform pH ranging from 7.9 units to 8 units and Ω_{Ar} that only varied from 1.25 to 1.5 units south of 45˚S. The highest Ω_{Ar} of 2.2 in the ESACW near 40˚S and the relatively low pH and Ω_{Ar} in AAIW were also remarkable in spring. The winter gradients of pH and Ω_{Ar} extend down to 1000m and the water column in winter is more variable, with highest pH (8.3-8.4 units) and Ω_{Ar} (3.2-3.4 units) in the northernmost part (north of 45˚S) although the highest values of Ω_{Ar} were only found near the surface (above 400m).The lowest winter pH (7.8-7.9 units) and Ω_{Ar} (1) values were found in the UCDW (south of 55˚S) below 400m. High values of pH (8.2-8.3 units) and Ω_{Ar} (2.2-2.4 units) were found in the AAIW (at the surface of 50˚S) and near the WW (at the surface of 60˚S).

4. Discussion

This work was designed to study the seasonal contrasts in the meridional gradient at the surface and the upper 1000 m of the carbonate system in the Southeast Atlantic sector of the Southern Ocean. While the climatological characteristics of meridional carbonate gradients are well established (Wu *et al*., 2019; Liu and Tanhua, 2019), there is still a significant gap in observing and analyzing the seasonal characteristics of the meridional gradient outside the Drake Passage, particularly in the S.E Atlantic Ocean (Munro *et al.*, 2015; Fay *et al.*, 2017).

The study is confined to the seasonality of the surface and upper 1000m of the upper cell of the MOC (Figure 5) (Sarmiento and Gruber, 2006; Marshall and Speer, 2012; Egan *et al.*, 2013). In the Southern Ocean, the strong meridional gradients of physical and carbonate characteristics of surface waters are largely determined by the formation (AAIW, SAMW) to the north of the Polar Front and outcropping (CDW) of water masses to the south of the PF (Marshall and Speer, 2012; Wu *et al.*, 2019; Liu and Tanhua, 2018) (Figures 9 & 11).

4.1 The seasonal surface meridional oceanographic characteristics

The results from this study defined three main water masses at the surface in winter and in spring; Eastern South Atlantic Central Water (ESACW), Antarctic Intermediate Water (AAIW) and the Antarctic Surface Water (AASW) through t-S diagrams (Fig 9) and Table 1. Both the winter cooling and wind action are responsible for the formation of ESACW that we identified at the surface largely confined to the density anomaly of 26-26.5 kg/m^3 and t, S characteristics 7.5-15˚C, 34.3-35.4 (Figure 9). The surface layer t, S characteristics (Figure 9) are consistent with the climatological meridional gradients with very small differences between winter and spring in the meridional gradients of sea surface temperature (SST) and sea surface salinity (SSS) evident in Fig (10); with lowest surface temperatures at high latitudes and highest temperatures in the north at the Sub-Tropical Front (S-STF) where there is greater exposure to solar heating in the mid-latitudes with SST (>10˚C) and SSS (>34.5) near S-STF (Fig 10) which are consistent with the properties of ESACW (Fig 9).

The seasonal differences are highlighted with more granularity in Fig (10) where strong meridional gradients and sharp fronts are shown with greater level of detail. The SSS gradients are comparable across both seasons, with a salinity minimum at 45˚S-50˚S (PFZ), a gradual increase to the south

and a sharp increase to the north (Fig 10). The PFZ marks the change in the balance of stratification from approximately equal contributions of salinity and temperature to stratification (north of PFZ) to salinity-dominated stratification south of PFZ (Palter *et al.*, 2013).

As expected, to the south of the SAF (from SAF to SBdy), the winter SST is slightly and consistently cooler than in spring (by 0.71˚C, 0.67˚C and 1.2˚C from SAF to PFZ, PFZ to SACCF and SACCF to SBdy respectively) and the SSS is slightly and consistently saltier in winter than in spring (by 0.03, 0.06 and 0.04 from SAF to PFZ, PFZ to SACCF and SACCF to SBdy respectively). This suggests that SST seasonal differences are comparatively more evident (mean seasonal difference of 0.86˚C) than the seasonal SSS differences (mean difference of 0.04). To the north of the SAF (from SAF to STF), the winter SST is 2.12˚C lower than the spring SST but the SSS is slightly fresher (by 0.18) in winter than in spring. These findings are consistent with what we observed south of SAF in that the SST seasonal differences are relatively more notable while the SSS seasonal differences are smaller ($0.18 << 2.12$˚C).

In Fig 10 (See also A1), small seasonal differences in surface salinity are evident where winter SSS is higher than spring SSS by ± 0.02 at the beginning of mid-latitudes (40-42˚S) and by ± 0.11 at the end of higher latitudes (55-56˚S). In both ends of the meridional gradient, surface salinity is highest because of the processes that occur in these regions. The saltier winter waters can be attributed to upwelling of saltier CDW as well as Ekman advection of higher salinity polar surface waters from sea ice formation (Ren *et al*., 2011). During the course of autumn and winter when sea ice forms and grows thicker, this happens south of SBdy but the elevated salinity water is then advected north by Ekman thus increasing the salinity of surface waters south of PFZ and winter water that it is released into (Jeffries., 2021). Surface salinity is lower at high latitudes in spring and summer because seawater is diluted by freshwater from sea ice thaw (Jeffries, 2021). The higher salinity values in the southerly fronts (SACCF and SBdy) associated with the meridional gradient of SSS are attributed to the impact of the upwelled CDW of deep, salty water (González-Dávila *et al*., 2011; Wu *et al.*, 2019).

The seasonal differences in the meridional gradient of salinity are clearer between SBdy and PFZ where spring is about 0.05 fresher than winter, thus resulting in spring SST that is 0.94˚C warmer than winter SST in that region (Figure 10b). In the high latitude (south of the PFZ), salinity plays a critical role in controlling stratification to form a shallow surface layer that warms significantly even though solar heat flux is weaker (Haumann, Gruber and Münnich, 2020). The SO surface

freshwater flux balance is dominated by the sea-ice induced freshwater fluxes in the seasonal ice zone (Haumann, Gruber and Münnich, 2020). Therefore, these fluxes are responsible for both surface freshening and for the temperature trends in high latitudes.

Surface freshening (in spring) in high latitudes is known to result in cooling by increasing the vertical density stratification in the upwelling region, and thus reducing the amount of deep, warmer waters entering the surface layer (Haumann *et al*., 2020), this is another reason for colder higher latitudes (further south of PFZ) compared to mid-latitudes. The maximum precipitation due to rain or snow peak may be responsible for salinity minimum at the PFZ (Fig 10b) (Liu and Tanhua, 2019). North of the PFZ however, the seasonal differences in SST are dominated by the spring-summer heat flux (Fig 10a).

In summary, while the seasonal physical oceanographic surface characteristics, in winter and spring are comparable in terms of the meridional gradients of SST and SSS, there are small but significant seasonal state differences particularly south of the PFZ (Fig 10a and b) where spring SST was about 0.67˚C and 1.2˚C warmer than winter SST from PFZ-SACCF and from SACCF-SBdy zones respectively. The spring SSS was fresher by 0.06 (PFZ-SACCF) and 0.04 (SACCF-SBdy). Therefore, the seasonal contrasts in the surface layer physics (SST and SSS) are as expected.

4.2 The seasonal surface meridional carbonate characteristics

Expected C_T and A_T meridional gradients based on SSS and SST meridional gradients.

The A_T:

The A_T is typically correlated to SSS (Lee *et al.*, 2006; Carter *et al.*, 2016). Therefore, the A_T gradient is expected to increase gradually to the south of PFZ with A_T minimum at the PFZ and a sharp increase to the north of PFZ (Figure 10b).

The C_T:

Based on the SST gradient and water mass gradients that decreased meridionally from north to south (Figure 9; 10a), the C_T is expected to have a gradient increasing meridionally from north to south because the relatively warm waters further north carry less CO_2 while the southernmost waters hold more CO_2 due to upwelling of deeper CDW and more CO_2 solubility (Wu *et al.*, 2019).

Expected seasonal differences in C_T and A_T based on SSS and SST seasonal differences

Since the SSTs were comparatively lower in winter than in spring (Table A11), we expected higher C_T values in winter since there is more CO_2 solubility in colder waters (Wu *et al.*, 2019). We did not expect much seasonal difference in A_T because the seasonal SSS differences were insignificant (Table A11) (Figure 10b).

4.2.1 Comparative meridional gradients for C_T and A_T

The meridional gradients of C_T and A_T reflect the large-scale meridional oceanographic processes (Figure 11; Wu *et al.*, 2019). As expected, we see consistency between SSS and A_T gradients. That is why minimum A_T is as expected at the PFZ where we observed SSS minima. The oceanographic consistency between A_T and SSS consolidates the idea that the predominantly salinity linked interpolation methods such as Lee and LIARv2 (Lee *et al.*, 2006; Carter *et al.*, 2016) hold in this part of the system.

The meridional gradient of C_T is similar in both seasons; it is a meridional gradient that increases continually from STF in the north to SBdy in the south (Figure 11). The cooler SSTs in higher latitudes increase CO_2 solubility and the upwelling of CDW results in higher poleward C_T (Wu *et al.*, 2019; Cai *et al.*, 2020). The analysis from Wu *et al* (2019) reveals that the surface C_T from the global ocean also increases poleward, being positively related to latitude and inversely correlated with SST. Our study revealed similar results that showed a consistent meridional poleward increase of C_T between 40 and 57˚S while SST decreased meridionally from north to south (Figures 10, 11).

4.2.2 Seasonal differences in the magnitudes of C_T and A_T

The paradox of this data set is that we expected higher C_T in cold winter waters. The reason why we expected higher C_T in winter is that lower temperatures in winter would result in greater solubility of CO_2 (Wu *et al.*, 2019), but the opposite was observed (Figure 11a). It was remarkable to discover that where we observed slightly high SST (Spring) there is high C_T and where we found slightly low SST (Winter) there is also low C_T (Figure 11a). The C_T is consistently higher in spring than in winter from STF near 40˚S to SBdy near 57˚S (Figure 11a), with the mean seasonal differences of 5.86µmol/kg, 21.9µmol/kg, 17.33µmol/kg and 15.89µmol/kg within the zone

boundaries STF-SAF, SAF-PFZ, PFZ-SACCF and SACCF-SBdy respectively (Table A12). These higher spring C_T values were observed even though we observed higher SSTs in spring and have already established that there is an inversely proportional relationship between SST and C_T gradients (Figure A2). So, our observations are not in agreement with the theory that suggests that C_T and SST are inversely correlated (Wu *et al.*, 2019).

Given that there is not much of a seasonal difference in salinity, we did not expect much seasonal difference in A_T. Our results revealed comparable meridional gradients but counterintuitively, C_T was higher in spring than in winter. This study proposes three explanations for higher C_T in spring than in winter:

1. Seasonal CO_2 equilibration lags heat flux so although the physics was seasonally consistent (SST), the C_T was lagging.
2. Winter cruise was still late autumn with later Primary Production which sustained decreased C_T even if SST had decreased.
3. Ship sampling bias - respiration in the sea water supply which is temperature dependent led to more C_T in spring.

The seasonal lag explanation: C_T (CO_2) exchanges were slower than heat and lag temperature (heat fluxes) changed by a few months and did not catch up and increase when the SST dropped in winter. This suggests that the results of that "catch up" were only measured in our spring cruise when surface warming had already started but CO_2 still reflected the winter concentrations (Figure 11a). So, although it was starting to warm up, the C_T was still that of winter. The reason for temperature and CO_2 cycles to be slightly out of phase (Fig 9 and 11) is that while temperature is largely controlled by air-sea fluxes, the CO_2 is largely controlled by the winter entrainment in the mixed layer deep ends because of convective overturning (Williams *et al.*, 2018). Also, there is a progressive increase in the Mixed Layer Depth (MLD) as you slide out of summer into winter and as the mixed layer deepens in winter, the C_T increases due to upwelling (Williams *et al.*, 2018) and peak of the mixed layer depth typically occurs in August and September (Holte and Talley, 2009).

The biogeochemical lag explanation: The seasonal period of gas exchange processes is longer (months to seasonal) than the period of biological production which only lasts for weeks-months (Cai *et al.*, 2020) so it is possible that the reason for winter C_T to remain low even though SST had

decreased, was because in the "winter" we measured C_T that was still being depleted by phytoplankton from late autumn. Similarly in spring our observations may have preceded the spring bloom. So, the biogeochemical process that happened while we were sampling is the possible reason why the data from Winter reflected tail end autumn because the cooler winter water was being modified by primary production since continued autumn primary production can still occur even if MLD are deepening and light is decreasing. This may also be because in early winter, nutrients may be allowed to enter the upper mixed layer when the deep MLD penetrates the nutricline thus increasing the phytoplankton biomass while light conditions still support PP (Hou *et al.*, 2022).

The respiration explanation: Respiration in the underway seawater supply lines in the ship may lead to oxygen deficits of up to 4µmol/kg (Juranek *et al.*, 2010). We ran an experiment to test the impact of respiration in the supply of underway seawater and then compared the C_T and A_T data from CTD collected simultaneously at 10m with the data from the underway lab seawater supply. We found that both A_T and C_T from the underway system were only higher by 0.86 and 1.7µmol/kg respectively (Table A13). Since 1.7µmol/kg is far less than the mean seasonal differences that showed that spring C_T was 5.86 µmol/kg, 21.9µmol/kg, 17.33µmol/kg and 15.89µmol/kg higher than in winter within all the zonal regions that we identified, it is not likely that there was ship sampling bias caused by respiration in underway seawater supply. The first two explanations are still more likely to be possible explanations for higher C_T in spring than in winter. So, we cannot reject options 1 and 2 but we do not have enough data to constrain each one. It is likely that each one plays a role, even if it is small.

4.2.3 Processes for A_T

Although the meridional A_T gradients reflect the SSS gradients, these gradients are not perfectly correlated because A_T is also partially biologically cycled (Wu *et al.*, 2019). The alkalinity is also increased by biological consumption of nitrate (and other species like phosphate and sulphate) and denitrification since nitrate consumption is stoichiometrically linked to the removal of nitric acid which decreases the concentration of H^+, thus increasing A_T (Fry *et al.*, 2015). When upper ocean stratification is increased during warming, the upward nutrient supply to subtropical surface waters would also be reduced, thus impeding primary production (Hastings, 2021; Sarmiento *et al.*, 2004; Fripiat *et al.*, 2021).

However, when upward supply of nitrate is reduced, the composition of the phytoplankton community may be driven to shift towards smaller cells that specialize in reduced nitrogen assimilation. This would result in enhanced recycling since there would be longer and less sufficient food chains (Hastings, 2021), possibly leading to enhanced A_T. The A_T is decreased by nitrification (generation of nitrate) and the subsequent remineralization (Fry *et al.*, 2015). The surface A_T concentrations are also increased by convective mixing and entrainment of A_T -rich deep waters during seasonal cooling (Lee *et al.*, 2006). During seasonal warming, the surface A_T may also be reduced as a result of shoaling of the mixed layer which reduces the contribution of the deep waters rich in A_T (Holte and Talley, 2009).

4.2.4 Processes for C_T

Deep ventilation that takes place south of PF results in deep waters that are rich in C_T and A_T (Wu *et al.*, 2019). This is supported by Fig 11 which showed increasing gradients of A_T and C_T south of PFZ. The increase in C_T could also be a result of the solubility pump which is based on the idea that higher latitudes have high C_T because the CO_2 solubility is increased in waters with lower temperature (Wu *et al.*, 2019; Cai *et al.*, 2020). Thus, surface C_T meridional distribution is primarily controlled by temperature, water masses and A_T that is why surface waters at low latitudes/in warm regions i.e ESACW hold less C_T while surface waters at high latitudes/in cool regions i.e AASW hold more C_T (Wu *et al.*, 2019). The A_T regulates surface C_T by setting equilibrium capacity of seawater to store C_T in solution; so, we attributed the C_T trend to upwelling of A_T-rich deep water at high latitudes (Fig 11b).

The study of Wu (2019) pointed out that the C_T trend was not primarily driven by A_T (it is not a dominant driver) since their study observed low A_T values in higher latitudes. We found that the A_T was generally high in both ends of our A_T gradient, that is, in higher latitudes near SBdy and near STF (Figure 11b). The A_T decreased while C_T increased at the S-STF in both seasons, this is similar to the study of González-Dávila *et al* (2011) which further explained that at the time of their cruise, the upwelling of CO_2-rich waters took place in this frontal area. The study of Wu (2019) deduced that since equilibrium C_T is changed by upwelling A_T, the upwelling of A_T is therefore crucial in shaping the spatial distribution of surface C_T. This may explain why the ratio of C_T and A_T is 1:1 south of 50˚S (Figure A3; Table 2).

The biological carbon drawdown in warmer seasons and mixing of C_T-rich deep waters are also responsible for the seasonal differences in carbonate parameters (Wu *et al.*, 2019). The distribution of surface C_T can be affected by the direct and indirect processes. The processes that influence the direct addition or removal of C_T include the entrainment of C_T-rich waters from the bottom of the ocean to the surface; Remineralization which leads to C_T release; primary production which leads to biological carbon assimilation as well as production and export of $CaCO_3$. The $CaCO_3$ also influences A_T, its dissolution increases A_T while its formation reduces A_T (Figure 4). Processes that result in indirect addition and removal of A_T and C_T include seawater concentration or dilution due to evaporation or precipitation (Wu *et al.*, 2019).

4.3 Seasonal and meridional differences in the pH and carbonate saturation (Ω_{Ar})

The meridional differences in pH and Ω_{Ar} based on SST and SSS meridional gradients

The pH and Ω_{Ar} gradients were both expected to decrease meridionally from north to south in winter and spring because they are driven by $[CO_3^{2-}]$, which would be expected to be inversely correlated to the C_T gradient (Equations 9&10). The other driver of low saturation is cold water (Chierici and Fransson, 2009) and we have shown that the SST decreased with increasing latitudes (Figure 10a) so Ω_{Ar} is expected to decrease meridionally with increasing latitude. The relationship between CO_3, pH and Ω_{Ar} are summarized by equations 9 and 10 below:

$$H^+ = K_2 * HCO_3/CO_3 \quad (9)$$

$$\Omega_{Ar} = CO_3/CO_{3sp} \quad (10)$$

4.3.1 Uncoupling of the meridional gradient of pH and Ω_{Ar}

One of the striking results from this study are the differences in the meridional gradients of pH (weak) and Ω_{Ar} (strong) (Figures 12a, b). These gradients appear uncoupled (Figures 12a, b). The Ω_{Ar} meridional gradients respond as expected to the meridional gradient of the ratio of C_T:A_T associated with ocean circulation, upwelling of CDW, and meridional cooling. However, pH does not (Figure 12a). Rather, apart from frontal excursions, it remains steady, ranging from 8.02 to 8.13 in winter and 7.99 to 8.09 in spring (0.06 units higher in winter than in spring) from 40˚S to 57˚S (Figure 12a).

The reason for the uncoupled gradients of pH and Ω_{Ar} can be explained by exploring the effect of the SST meridional gradient on the carbonate system properties since the chemical equilibrium (K_0, K_1, K_2) is sensitive to temperature such that a decrease in SST leads to decreasing K_2 (Figure A5). However, as the SST decreases, the ratio of HCO_3/CO_3 is increasing (Figure A5). So, the impact of SST on K_2 cancels the impact of C_T on the HCO_3/CO_3 ratio which uncouples the meridional gradients of pH and Ω_{Ar}. The effects of temperature also work to enhance each other for C_T and $[CO_3^{2-}]$ whereas they counteract each other for pH and $[H^+]$ during cooling (Cai *et al.*, 2020).

The significant impact of SST on pH and Ω_{Ar} gradients is confirmed by how the differences in meridional gradients of pH and Ω_{Ar} (Figure 12) disappeared when a constant temperature was used, and it is worth noting that the gradient of Ω_{Ar} remained the same (Figure A4). The pH gradient changed due to a thermodynamic equilibrium shift (Cai *et al.*, 2020). The $[CO_3^{2-}]$ declined meridionally (thus decreasing Ω_{Ar}) since more CO_2 was retained in upwelling waters as shown by increasing C_T and A_T gradients in higher latitudes (Figure 11) and outcropping of water masses (Figure 9). Biological CO_2 removal is another driver of relatively higher pH in the mid latitudes than in higher latitudes. This shows that there is a distinct sensitivity of pH and Ω_{Ar} to biological processes, gas exchange, thermodynamic constants and mixing (Cai *et al.*, 2020).

The equilibria between carbonate species shifts towards increasing carbonate ion concentration when temperature increases (Wu, 2019). That is why there is relatively higher $[CO_3^{2-}]$ and thus higher Ω_{Ar} in spring than in winter (Figures A6&A7) when constant C_T and A_T were used to derive $[CO_3^{2-}]$ and Ω_{Ar}. This is further supported by the Figures A8&A9, showing that $[CO_3^{2-}]$ and the CO_3/CO_{3sp} ratio (Ω_{Ar}) decrease meridionally due to decreasing SST when constant C_T and A_T were used.

The expected seasonal differences in pH and Ω_{Ar}

The persistent, strong winter winds as well as cooling in higher latitudes result in C_T-rich, carbonate poor deep waters (low Ω_{Ar}) whereas carbonate ion concentration is enriched (high Ω_{Ar}) in spring when shallow mixed layers evolve (González-Dávila *et al.*, 2011). But since our observations revealed that the C_T-rich waters were observed in spring, we expect higher Ω_{Ar} in

winter than in spring. The pH and Ω_{Ar} are determined by changes in water mass salinity and temperature through changes in C_T and A_T (Tynan *et al*., 2016). So, the derived [H^+] values are sensitive to measured C_T and A_T such that large errors in pH can result from small errors in C_T or A_T (Clayton *et al*., 1995). Hence, the pH and Ω_{Ar} are expected to be higher in this winter when C_T was comparatively low (Figures 11, 12).

4.3.2 Seasonal differences in pH and Ω_{Ar} based on C_T and A_T seasonal differences

It is evident in our results that seasonal differences in pH and Ω_{Ar} are controlled mainly by C_T (Figures A6 & A7). That is why as a result of C_T entrainment in late winter, there is higher C_T (Figure 11) and thus lower pH in spring than in winter (Figure 12). The production of organic matter occurs in the sunlit, uppermost layers of the ocean (Spring) and is known to decrease both the concentration of C_T as well as the concentration of free protons [H^+] thus increasing the pH in spring (Sarmiento and Gruber, 2006). However, the surface pH and Ω_{Ar} are unexpectedly higher in winter than spring since we found higher C_T in spring. That may be because the timescale of the physical and biological processes is different from the timescale for air-sea equilibrium of CO_2 which takes about six months (Sarmiento and Gruber, 2006).

The physical processes such as mixing and upwelling act on a timespan of days to weeks, the timescale of biological production is also weeks while the period of gas exchange processes is months to seasonal and the thermal cycle is also seasonal (Cai *et al.*, 2020). Thus, spring lagged the winter signal and winter lagged the autumn signal. The pH and Ω_{Ar} seasonal differences are consistent with the "late season" hypothesis that was stated above.

To summarize, in the absence of significant differences in AT, C_T was the dominant driver of the seasonal differences in pH and ΩAr that is why surface pH and ΩAr are unexpectedly higher in winter than spring since we found higher C_T in spring. As a result of C_T entrainment in late winter, there is higher C_T and thus lower pH in spring than in winter. This C_T entrainment in late winter is what drove the CO_2 but temperature was driven by air-sea fluxes of heat hence CO_2 cycles and temperature were out of phase. So the explanation of pH and ΩAr seasonal differences is not different from the seasonal lag explanation; instead both this explanation and the biogeochemical lag explanation can be used to explain the seasonal differences in pH and ΩAr which were driven by C_T.

4.4 The seasonal oceanographic characteristics of carbonate system in the upper 1000m

This study has shown that the surface meridional gradients of A_T and C_T are sensitive to the outcropping of water masses (Figure 9; Figure 11). Here we want to investigate the seasonal contrasts in the carbonate system of the upper 1000m and what role they may play in the surface seasonality. The transformation of physical and carbonate properties over winter and spring will be analysed in a water masses framework. This will help us to better understand the seasonal dynamics of SO CO_2 uptake and release. For instance, anthropogenic CO_2 that enters the Southern Ocean across the air-sea boundary is eventually incorporated into Intermediate (AAIW) and mode waters (SAMW) (Marshall and Speer, 2012; Tanhua *et al.*, 2017).

The CO_2 is sequestered via the formation of these water masses in the northern part of the ACC; SAMW moving northward absorbs anthropogenic CO_2 and subducts to form the ESACW and AAIW that are separated from the surface layer near SAF (Figure 5; Tanhua et al., 2017). This is the main region where anthropogenic CO_2 is taken up and sequestered in the Southern Ocean (Tanhua *et al.*, 2017). Greater amounts of CO_2 are also trapped by the saltier Antarctic bottom waters in the deep ocean (Schmitt., 2011). However, the lower loop will not be discussed in this study because our observations end at 57˚S. Lower loop refers to the southernmost part of the lower cell of the global meridional overturning circulation in the Southern Ocean (Figure A15).

4.4.1 Physical properties of the water masses

The characterization of the physical and carbonate properties of water masses (Figure 13) has been improved by the recent high-resolution observations from south of Africa in the Atlantic Ocean (González-Dávila *et al*., 2011; Liu and Tanhua, 2019; Orsi *et al*., 1995). Here we build on this work by enabling a seasonal comparison of the physical and carbon state properties in the upper 1000m in support of the analysis of the surface gradients (Figures 14, 15, 16 and 17). The distribution of five main water masses was shown through the SE. Atlantic basin: The ESACW, AAIW, WW, AASW and the UCDW (Figure 13). In addition to salinity and temperature, density was also used for their characterization (Table 3). The t-S diagram revealed strong similarities between winter and spring, with AASW and the AAIW being expectedly the fresher waters (Figure

13). The increased salinity near STF in the ESACW in spring is consistent with the surface gradient of SSS as is the salinity minimum in the vicinity of the Polar Front zone (Figs 10, 14).

During the formation of ESACW, the South Atlantic Current from the west (McCartney., 1977) meets and mixes with water brought from the Indian Ocean by the Agulhas Current (Liu and Tanhua, 2019). This mixing occurs southwest of South Africa in the eastern South Atlantic Ocean (Liu and Tanhua, 2019). Most of the resulting ESACW water forms a deep mixed layer through winter cooling and is subducted along the isopycnal surfaces by Ekman pumping and is eventually injected into the ocean interior (Tomczak, 1999).

The potential density of ESACW is within the range of 26.00 and 27.20 kg/m^3 as in the study of Liu & Tanhua (2019). Their study also revealed a linear T-S relationship across that range of potential density; this pattern was also observed in this study for both seasons (Fig 13). The central water mass ESACW is identified by high salinity, the excess salinity that is observed in the ESACW domain could be attributed to the Agulhas current which has high salinity because of evaporation in the subtropics (Ríos *et al*., 2003) while formation of AASW fresher-cold layer over the AAWW might be the reason for low salinity values near the surface (Figure 14b).

The AAIW, characterized by a salinity minimum from excess precipitation in the Polar Front zone, sinks into intermediate depth (600-800m) after formation in the shallow layer. (Fig 14b and 16c)(Liu and Tanhua, 2019). In both winter and spring, the AAIW is within the density anomaly range of 27.00-27.10 kg/m^3 and 27.40 kg/m^3 as in the study of Liu & Tanhua (2019). The distribution and transport of intermediate water mass is significantly influenced by the currents in the intermediate layer. The AAIW is fed by the near-surface water of the APZ as it subducts northward at the SAF (±45˚S) (González-Dávila *et al*., 2011). This near-surface water is considered the least saline in the ACC band, that is why the AAIW has the minimum salinity (Fig 13). Formation of AAIW was observed in both winter and spring but it was stronger in the latter where salinity minimum extends down to 600m, this points to seasonal inertia in the upper 1000m (Figure 14b).

In the Southern Atlantic, the upwelling of deep waters occurs along the density isopycnals of 27.6 and 27.9 kg/m^3 (Wu *et al.*, 2019); our results reveal that the water masses with this density are the UCDW (Figure 13). Since this water mass is found further south, It has comparatively low temperatures, higher salinity and higher densities (Figure 13). In fact, CDW is characterized by a

potential density larger than 27.8 kg/m^3 in the study of Liu and Tanhua (2019). The potential density of CDW from our study is greater than 27.6 but less than 28 kg/m^3.

The extensive mixing of CDW with AAIW, ESACW AWW and AASW is happening south of PFZ as shown by the circle in Figure 13. Although Figure 14 shows the typical distribution of temperature and salinity at the top 1000m, it also shows seasonal contrasts, the most evident being the increased temperature and salinity near the surface of the northern boundary 40-42˚S in spring. These characteristics may be attributed to the presence of the frontal structure STF or Agulhas eddies in the northern edge where we identified the ESACW water mass in spring and not in winter. So, the main seasonal contrasts are the stronger temp and Salinity gradients in the northern SAZ (Figure 14).

There is a clear signal of UCDW from the high salinity in both seasons (Figure 14). The increase in salinity near 60˚S may also be a result of brine rejection during equatorward transport of sea ice and during sea ice formation in winter (Williams *et al*., 2018). The vertical distribution of salinity in winter can be attributable to the fact that the cold, saltier water sinks, resulting in higher salinity in the UCDW. The anomalies at the STF may be linked to the eddies that were crossed over at about 40-42˚S (Figure 15). The evidence of the anticyclonic eddy is not seen in winter whereas the cyclonic eddy that was crossed in spring is carrying water with the characteristics of ESACW as seen in spring.

4.4.2 Seasonal carbonate oceanographic characteristics

The carbonate seasonal properties of the upper 1000m in the oceanic region between the Antarctic and the African continent have not been fully explored (González-Dávila *et al*., 2011). This section discusses this gap and their consistency with the surface carbonate meridional gradients (Figures 11a&b, 16 and 17). The A_T sections obtained from the linear interpolation LIARv2 method, are expected to be consistent with the salinity sections while C_T sections are expected to resemble the temperature sections.

The seasonality in export production as well as the seasonality in wind stress both influence the seasonal cycle of C_T: The upwelling of the C_T-rich water is enhanced by the strong wintertime westerlies whereas upwelling is inhibited by the relatively weak summertime westerlies (Conrad and Lovenduski, 2015). The influence of winds on A_T is the same as that on C_T, so there should be

lower surface A_T in summer and higher surface A_T in winter. Instead, we observed higher surface A_T near high latitudes in spring than in winter (Fig 16). Similarly, the decrease in surface C_T is driven by the export production in summer while the increase in surface C_T is driven by low export production in winter. However, there was more surface C_T reduction at 40-50˚S in winter than in spring (Fig 16) although the temperatures in this region were higher in spring (Figure 14). The lag effect from winter to spring was not only seen at the surface but also in the interior, growing up to 1000m; this shows that these seasonal differences were driven by physical factors such as vertical mixing.

The vertical sections of A_T and C_T show more C_T and A_T in the UCDW while ESACW have low C_T and A_T minima is observed in the AAIW (Figure 16). Isopycnal outcropping of water masses occurs near the Antarctic continent where CDW derived from North Atlantic Deep Waters (NADW) from the north Atlantic Ocean enters the Southern Ocean at high densities ranging from 27.75-27.85 kg/m^3 (Marshall and Speer, 2012). The wind stress is greatest in the Antarctic Circumpolar Current (ACC) so upwelling occurs within this domain (Wu *et al.,* 2019) hence we see A_T-rich and C_T-rich UCDW being carried to the surface south of 50˚S (Figure 16).

Ekman transport in the surface layer is responsible for northward advection of upwelled waters which then fuel primary production and thus carbon export (Egan *et al.,* 2013) resulting in lower A_T and C_T further north where primary production is promoted. Some of the upwelled water travels southward to close the "lower loop" while some of it moves into the intermediate depths and provides nutrients to the lower-latitude thermocline; this nutrient supply will then determine the degree of carbon export outside the Southern Ocean (Egan *et al.,* 2013). The increased C_T in CDW (Figure 16c) also results from the old waters from Pacific and Indian Oceans (González-Dávila *et al.*, 2011).

Conrad and Lovenduski (2015) found that the seasonal cycle of carbonate ions is less influenced by salinity and temperature while contributions from A_T and C_T are relatively more. The carbonate ion concentration (and thus Ω_{Ar}) is driven down by high surface C_T in winter, and it is driven up by low surface C_T in summer (Conrad and Lovenduski, 2015) but this is contrary to our results which revealed higher Ω_{Ar} values in winter than in spring (Fig 17b). The carbonate ion concentration is also driven up by high surface alkalinity in winter and it is driven down by low surface alkalinity in summer (Conrad and Lovenduski, 2015). As expected, the pH and Ω_{Ar}

gradients are similar. The lower pH in Figure 17 is associated with high C_T while higher pH is associated with low C_T and high A_T. In contrast to the winter system which is much more variable, the pH variability is much smaller in spring. This highlights the fact that there are very important seasonal contrasts in the upper 1000m. The gradient lines are vertical in winter but in spring the system is much more mixed, as a result of the isopycnal flow associated with it. The reduced pH and Ω_{Ar} in the AASW suggest that UCDW (with low pH and Ω_{Ar}) was the source of the water that was brought to the surface south of the polar front (Figure 17).

5. Synthesis and Conclusions

This study used surface and upper 1000m oceanographic observations from two seasonally distinct cruises in July/August (Austral Winter) and Oct/Nov (Austral Spring) 2019 to explore the seasonal differences in the meridional gradients of physical and carbonate characteristics i.e t, S, C_T, A_T, pH and Ω_{Ar}. This study drew three main findings from the seasonal contrasts in surface carbonate observations.

While the surface meridional gradients of C_T and A_T were comparable between seasons, the state C_T concentrations were found to be unexpectedly higher in the slightly warmer spring waters. The reverse was expected in winter when intensified convective mixing of C_T-rich deep waters occurs. There was an insignificant seasonal difference in A_T, which correlated strongly to Salinity, with maxima at the meridional extremes and a minimum in the PFZ.

This study proposed that while surface layer warming and cooling adjust quickly to seasonal changes in the net heat flux, there was a significant seasonal lag in the response of CO_2 related to the slower transfer velocities and the seasonal lag of the drawdown of CO_2 by surface primary production. Thus, from a carbonate system perspective, what was thought to be the winter season was in fact the tail end of autumn and what was considered to be spring was a lagged reflection of winter deep entrainment of elevated C_T. Finally, the study found that meridional gradients of surface pH and Ω_{Ar} were uncoupled. Whereas the Ω_{Ar} followed the meridional C_T-driven trend, apart from some frontal variability, the pH had no significant meridional gradient trend. This study attributed this to the impact of the meridional temperature gradient on the K_2 equilibrium constant which compensated for the impact of the C_T gradient on pH.

This study then compared the seasonal differences in the upper 1000m. It was found that winter A_T data were erroneous, so A_T was derived from the LIARv2 method for both winter and spring. A comparison of observations and the LIARv2 method in the spring provided confidence for the reconstruction in both spring and winter. It was found that the surface water gradient characteristics were coherent with the meridional physics and carbonate water mass characteristics. Although waters below 200 m would integrate over longer timescales, the interpretation of our data was from short time scale observations (winter-spring of the same year) but these observations showed that seasonality in carbonate system parameters was apparent down to 1000 m. The significant seasonal differences in temperature, salinity, C_T, A_T, pH and Ω_{Ar} suggests that the impact of the seasonal cycles was not just in the surface, but it stretched down to the interior (down to 1000m). Since the seasonal impact is not only in the upper 200m, it was not only attributed to primary production but also to physical processes such as vertical mixing.

The main seasonal difference in the oceanography of the upper 1000m include characteristics of ESACW that were identified only in spring. With the characteristics of ESACW that include high temperatures and high salinity (from evaporation), it is believed that the surface near 40˚S was receiving enough sunlight to support biological production. Hence, it was expected that the biological export of C_T from surface down to deeper parts of the ocean would be enhanced. However, we discovered that the most reduction of C_T from the surface occurred in winter when the surface temperatures were relatively cooler. The pH and Ω_{Ar} distributions also indicated that the system was more mixed in spring even though the westerly winds were expected to be weaker during that period. This supports the seasonal lag idea that winter was in fact a delayed autumn and spring was a delayed winter. So, the differences between the findings from the physics observations (temperature and salinity) and C_T, A_T, pH and Ω_{Ar} suggests that the heat, salt and carbon fluxes were influenced by different seasonal processes that extend at least to 1000m depth.

The overall finding is that the timing of the cruises does not reflect the expected winter and spring-summer seasonal conditions of carbonate in the SE Atlantic Southern Ocean. Rather, the winter cruise reflects the conditions for the end of autumn, this is evident in the results that revealed low C_T and high pH in winter. Similarly, the spring cruise reflects conditions for the end of the winter season as supported by the observed high C_T and low pH.

6. Appendix: Supplementary results

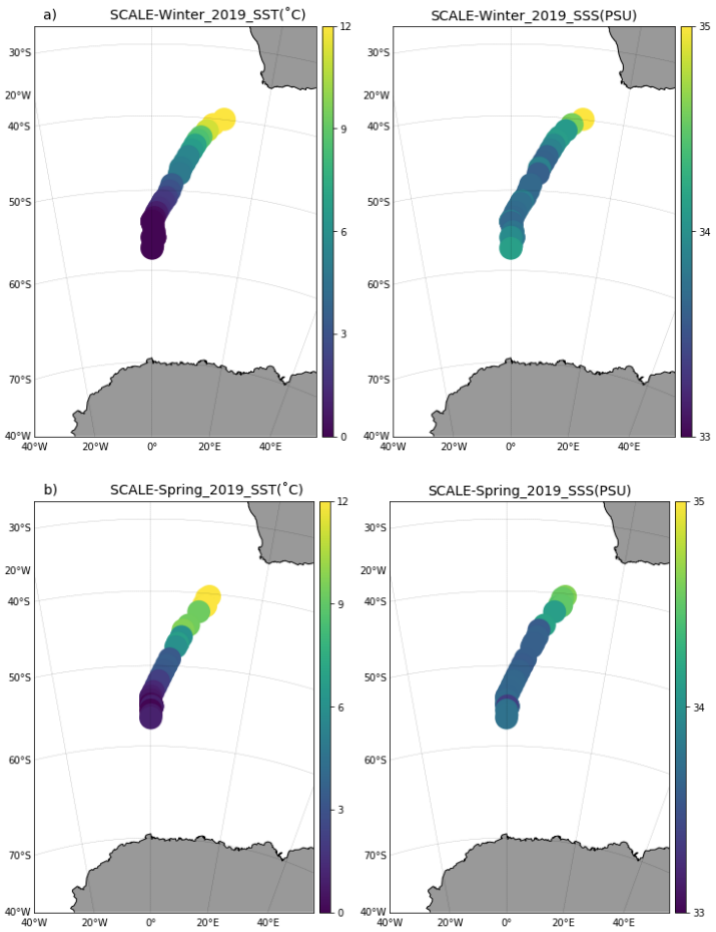

A1: Showing the temperature (˚C) and salinity of surface waters samples collected underway along the cruise track from the a) winter and b) spring SCALE cruises.

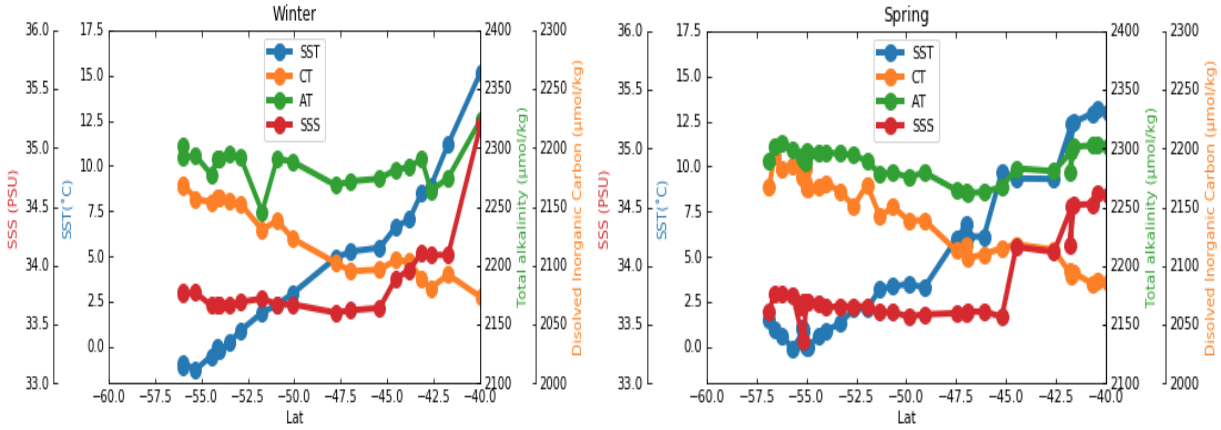

A2: Showing the relationship between SST, C_T, A_T and SSS in winter and spring

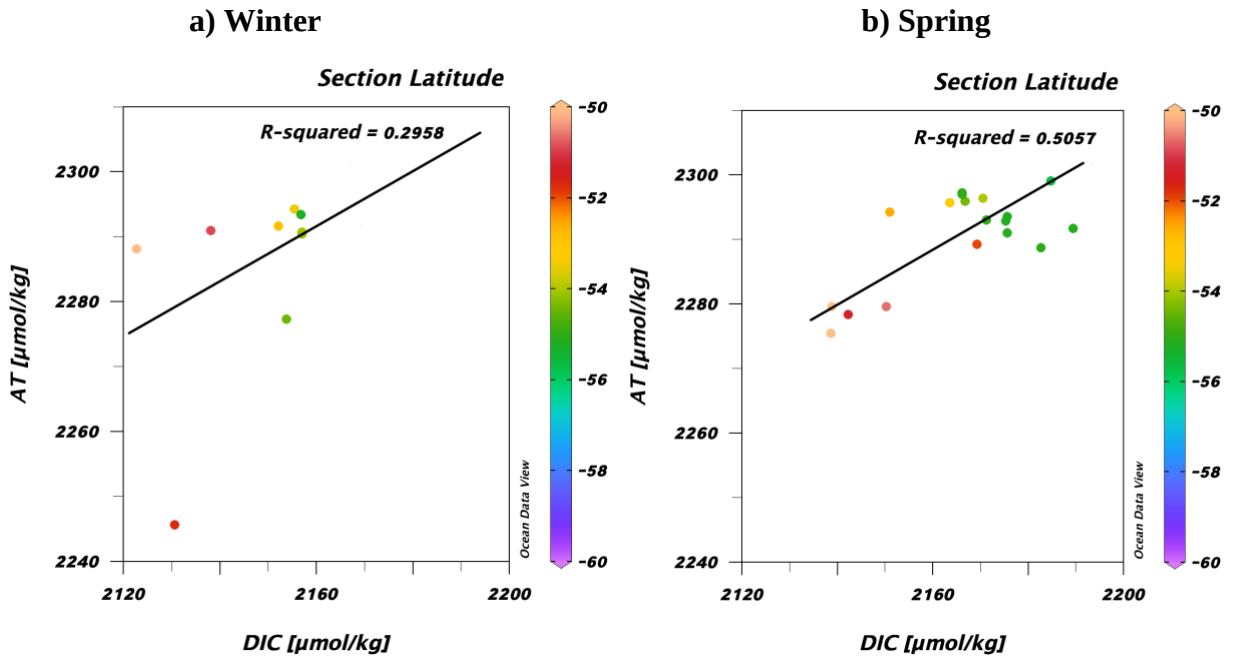

A3: The slope of dC_T/dA_T showing correlation between the surface C_T and A_T south of 50˚S in winter and spring where C_T:A_T ratio is 1:1. The regression equations are y = 0.02x+2275 and y = 0.01x+2273 for winter and spring respectively.

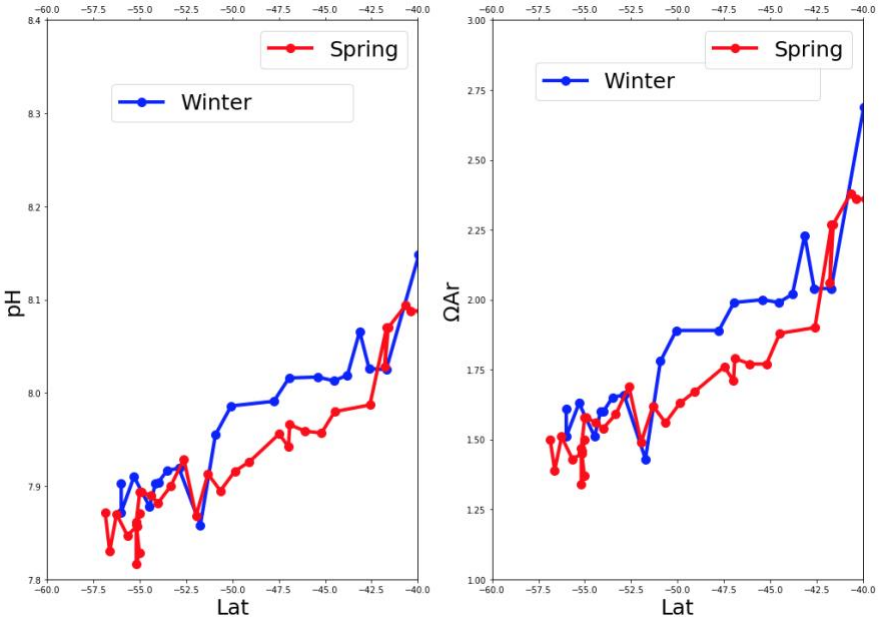

A4: Shows the pH and Ω_{Ar} gradients when a constant SST of 12˚C was used in the CO_2SYS calculations.

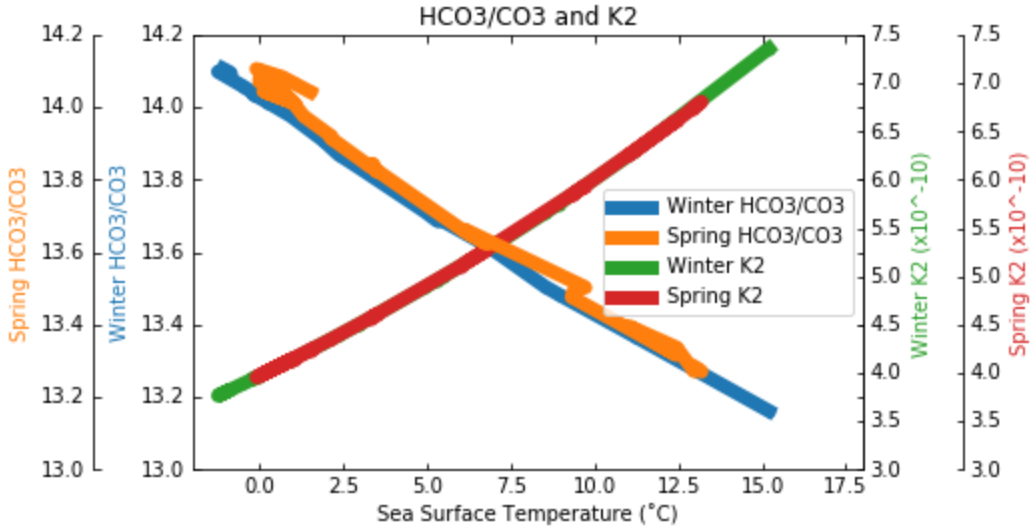

A5: The gradients of K_2 and HCO_3/CO_3 that were calculated using constant C_T and A_T values and in-situ SST

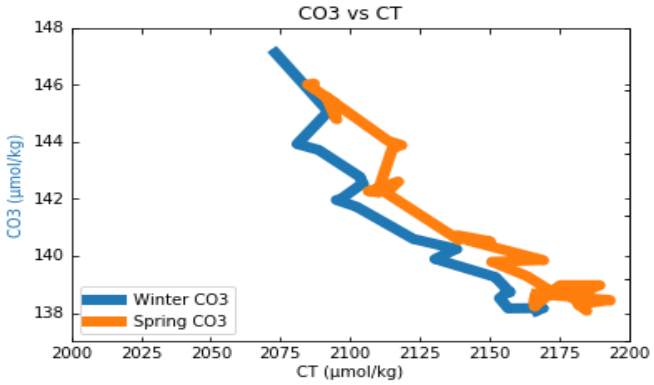

A6: Shows the CO_3 gradient against the C_T

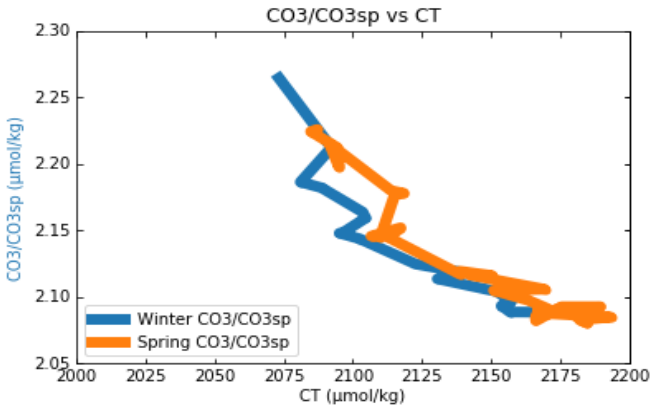

A7: Shows the gradient of the CO_3/CO_{3sp} ratio against C_T

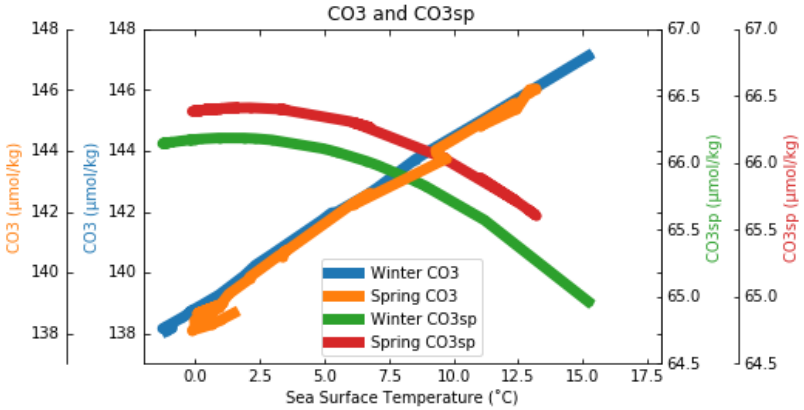

A8: The CO_3 and CO_{3sp} gradients against SST

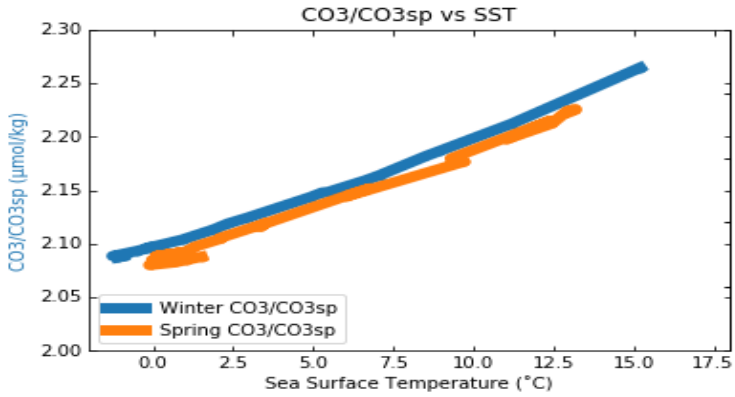

A9: The gradient of CO_3/CO_{3sp} ratio against SST

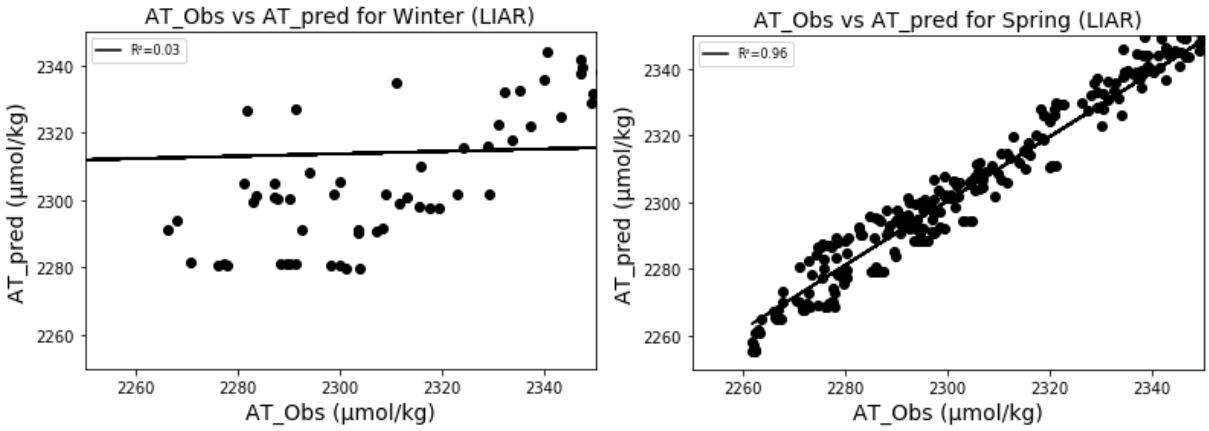

A10: The correlation between the predicted and the observed A_T values for a) winter and b) spring.

A11: Showing the averages of temperature and salinity that were measured from underway samples that are separated into sections using ocean fronts

Section	Winter (T; S average)	Spring (T; S average)	Diff (T; S average)
STF-SAF	9.59; 34.22	11.71; 34.40	2.12; 0.18
SAF-PFZ	5.23; 33.62	5.94; 33.60	0.71; 0.02
PFZ-SACCF	2.03; 33.69	2.70; 33.63	0.67; 0.06
SACCF-SBdy	-0.53; 33.71	0.67; 33.67	1.2; 0.04

A12: Showing the averages of C_T and A_T that were measured from underway samples that are separated into sections using ocean fronts

Section	Winter (A_T;C_T average)	Spring (A_T;C_T average)	Diff (A_T;C_T average)
STF-SAF	2286.30; 2090.55	2293.77; 2096.41	7.47; 5.86
SAF-PFZ	2271.23; 2098.05	2267.86; 2119.95	3.37; 21.9
PFZ-SACCF	2279.07; 2135.90	2285.38; 2153.23	6.31; 17.33
SACCF-SBdy	2291.29; 2159.47	2295.22; 2175.36	3.93; 15.89

A13: The C_T and A_T that were measured from underway samples vs those that were collected from CTD at the surface

	Underway samples	CTD surface (10m)	Mean difference
A_T average	2293.60	2292.74	0.86
C_T average	2140.66	2138.96	1.7
A_T STDev	0.84	0.57	
C_T STDev	3.70	3.07	

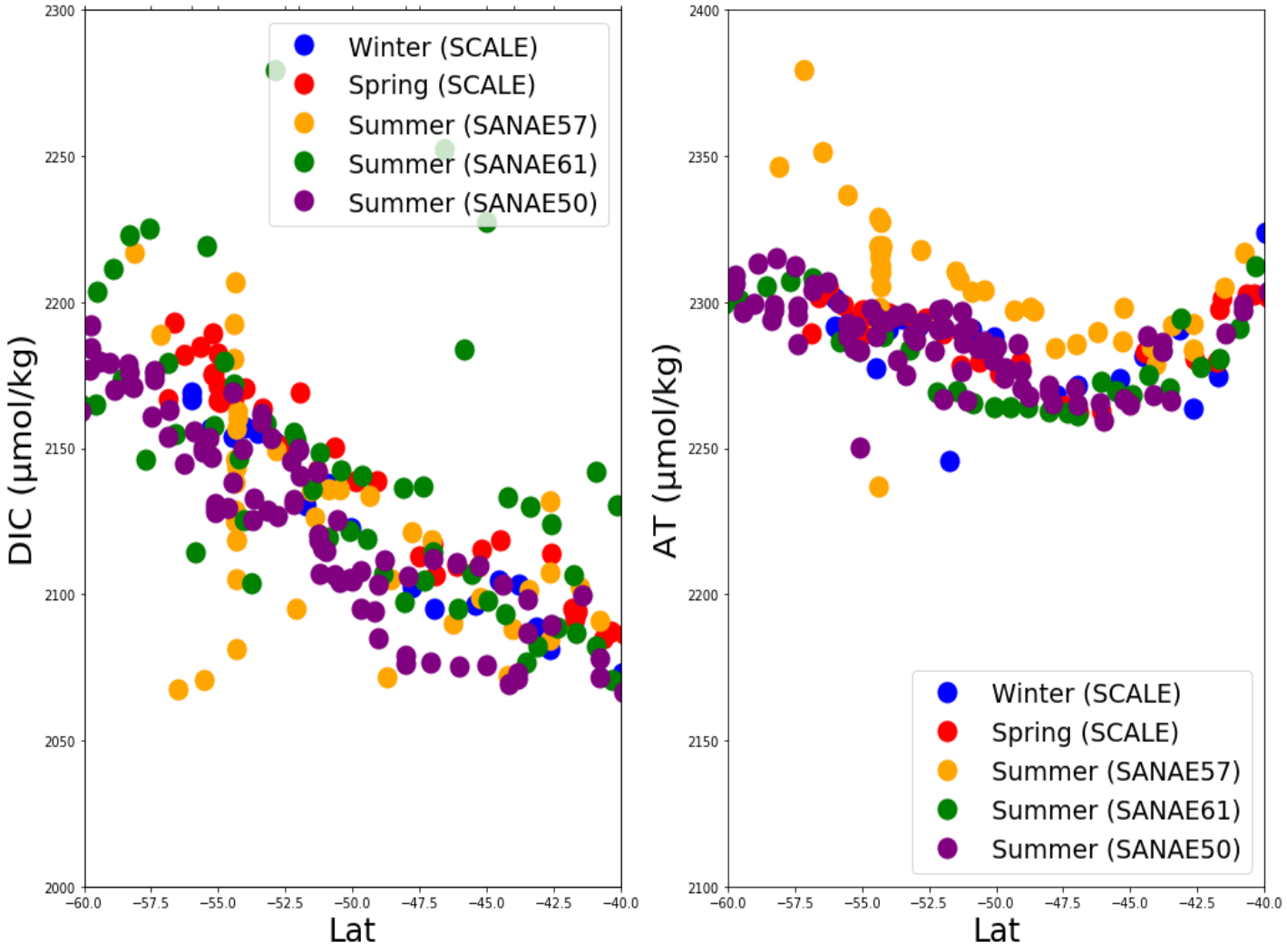

A14: The DIC and A_T meridional trends from SANAE summer cruises and the SCALE winter and spring.

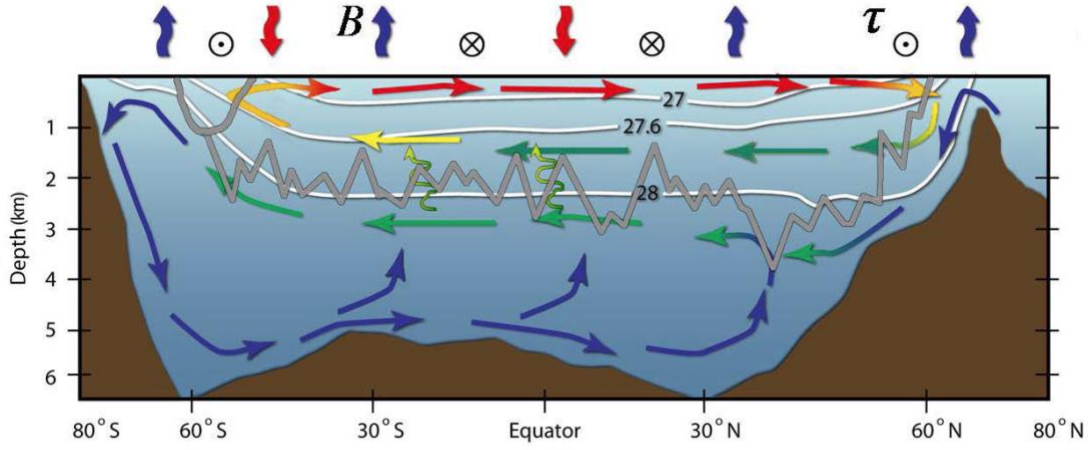

A15: The illustration of the Lower Cell and Upper Cell of the ocean's global meridional overturning circulation (Marshall and Speer, 2012).

7. References

Andrew, S. M. *et al.* (2019) 'Iron Availability Influences the Tolerance of Southern Ocean Phytoplankton to Warming and Elevated Irradiance', *Frontiers in Marine Science*, 6(November), pp. 1–12. doi: 10.3389/fmars.2019.00681.

Beaufort, L. *et al*. (2011) 'Sensitivity of coccolithophores to carbonate chemistry and ocean acidification', Nature, 476(7358), pp. 80–83. doi: 10.1038/nature10295.

Belkin, I. and Cornillon, P. (2003) 'SST fronts of the Pacific coastal and marginal seas', *Pacific Oceanography*,1(2),pp.90–113.
Available at: ftp://ftp.io.usp.br/lado_20130322/papers/belkin_cornillon_2003.pdf.

Bushinsky, S. M., Takeshita, Y. and Williams, N. L. (2019) 'Observing Changes in Ocean Carbonate Chemistry: Our Autonomous Future', Current Climate Change Reports. Current Climate Change Reports, 5(3), pp. 207–220. doi: 10.1007/s40641-019-00129-8. Bustos-serrano, H. (2010) 'The Carbonate System in Natural Waters', System, (August 2010). doi:10.13140/RG.2.2.27253.27369.

Byrne, R. H. (2014) 'Measuring ocean acidification: New technology for a new era of ocean chemistry',Environmental Science and Technology, 48(10), pp. 5352–5360. doi: 10.1021/es405819p.

Cai, W. J. *et al.* (2020) 'Controls on surface water carbonate chemistry along North American ocean margins', *Nature Communications*. Springer US, 11(1), pp. 1–13. doi: 10.1038/s41467-020-16530-z.

Cao, L. and Caldeira, K. (2008) 'Atmospheric CO_2 stabilization and ocean acidification', Geophysical Research Letters, 35(19). doi: 10.1029/2008GL035072.

Carter, L., McCave, I. N. and Williams, M. J. M. (2008) 'Chapter 4 Circulation and Water Masses of the Southern Ocean: A Review', *Developments in Earth and Environmental Sciences*, 8(08), pp. 85–114. doi: 10.1016/S1571-9197(08)00004-9.

Carter, B. R. *et al.* (2016) 'Locally interpolated alkalinity regression for global alkalinity estimation', *Limnology and Oceanography: Methods*, 14(4), pp. 268–277. doi: 10.1002/lom3.10087.

Chierici, M. and Fransson, A. (2009) 'Calcium carbonate saturation in the surface water of the Arctic Ocean: Undersaturation in freshwater influenced shelves', *Biogeosciences*, 6(11), pp. 2421–

2432. doi: 10.5194/bg-6-2421-2009.

Clayton, T. D. *et al.* (1995) 'The role of pH measurements in modern oceanic CO2-system characterizations: Precision and thermodynamic consistency', *Deep-Sea Research Part II*, 42(2–3), pp. 411–429. doi: 10.1016/0967-0645(95)00028-O.

Conrad, C. J. and Lovenduski, N. S. (2015) 'Climate-driven variability in the Southern Ocean carbonate system', Journal of Climate, 28(13), pp. 5335–5350. doi: 10.1175/JCLI-D-14-00481.1.

Coughlan, C. (2013) *Modelling the carbonate system to adequately quantify ocean acidification*. doi: 10.2788/57998.

Dickson, A. G. (2010) 'Part 1 : Seawater carbonate chemistry The carbon dioxide system in seawater : equilibrium chemistry and measurements', *Guide to best practices for ocean acidification research and data reporting*, (January), pp. 1–40. doi: 10.2777/66906.

Dickson, A. G., Sabine, C. L. and Christian, J. R. (2007) Guide to Best Practices for Ocean CO_2 measurements. PICES Special Publication, Guide to Best Practices for Ocean CO_2 measurements. PICES Special Publication.

Egan, K. E. *et al.* (2013) 'Opening the gateways for diatoms primes Earth for Antarctic glaciation', *Earth and Planetary Science Letters*. Elsevier, 375(November 2015), pp. 34–43. doi: 10.1016/j.epsl.2013.04.030.

Emery, W. J. (2015) 'Oceanographic Topics: Water Types and Water Masses', *Encyclopedia of Atmospheric Sciences: Second Edition*, pp. 329–337. doi: 10.1016/B978-0-12-382225-3.00279-6.

Emery, W. and Meincke, J. (1986) 'Global water masses: summary and review', *Oceanologica acta*, 9(4), pp. 383–391.

Fay, A. *et al.* (2017) 'Utilizing the Drake Passage Time-series to understand variability and change in subpolar Southern Ocean pCO₂', *Biogeosciences Discussions*, pp. 1–31. doi: 10.5194/bg-2017-489.

Fripiat, F. *et al.* (2021) 'Nitrogen isotopic constraints on nutrient transport to the upper ocean', *Nature Geoscience*. Springer US, 14(11), pp. 855–861. doi: 10.1038/s41561-021-00836-8.

Fry, C. H. *et al.* (2015) 'Analysis of global surface ocean alkalinity to determine controlling processes', *Marine Chemistry*. Elsevier B.V., 174, pp. 46–57. doi:10.1016/j.marchem.2015.05.003.

González-Dávila, M. *et al.* (2011) 'Carbonate system in the water masses of the Southeast Atlantic sector of the Southern Ocean during February and March 2008', Biogeosciences, 8(5), pp. 1401–1413. doi: 10.5194/bg-8-1401-2011.

Hastings, M. G. (2021) 'Reactive Nitrogen Cycling in the Atmosphere and Ocean', (May). doi: 10.1146/annurev-earth-083120-052147.

Haumann, F. A., Gruber, N. and Münnich, M. (2020) 'Sea-Ice Induced Southern Ocean Subsurface Warming and Surface Cooling in a Warming Climate', *AGU Advances*, 1(2). doi: 10.1029/2019av000132.

Henderiks, J. *et al*. (2012) 'Environmental controls on Emiliania huxleyi morphotypes in the Benguela coastal upwelling system (SE Atlantic)', 448, pp. 51–66. doi: 10.3354/meps09535.

Henriet, J.-P. *et al.* (2015) *Sailing Through Changing Oceans: Ocean and Polar Life and Environmental Sciences on a Warming planet*.

Hofmann, G. *et al.* (2015) 'Near-shore Antarctic pH variability has implications for the design of ocean acidification experiments', *Scientific Reports*, 5, pp. 1–10. doi: 10.1038/srep09638.

Holte, J. and Talley, L. (2009) 'A new algorithm for finding mixed layer depths with applications to argo data and subantarctic mode water formation', *Journal of Atmospheric and Oceanic Technology*, 26(9), pp. 1920–1939. doi: 10.1175/2009JTECHO543.1.

Ishii, M. *et al*. (2011) 'Ocean acidification off the south coast of Japan: A result from time series observations of CO_2 parameters from 1994 to 2008', Journal of Geophysical Research: Oceans, 116(6), pp.1–9. doi: 10.1029/2010JC006831.

Jeffries, M. (2021) 'Sea Ice | Formation, Extent, & Facts | Britannica', *Britannica*. Available at: https://www.britannica.com/science/sea-ice#ref908429.

Joncas, R. (2007) 'Introduction to the Guide', Stanford University, pp. 13–13. doi: 10.1007/1-56898-664-5_3.

Jones, J. M. *et al*. (2016) 'Evaluating carbonate system algorithms in a nearshore system: Does total alkalinity matter?', PLoS ONE, 11(11), pp. 1–12. doi: 10.1371/journal.pone.0165191.

Juranek, L. W. *et al.* (2010) 'Evidence of O2 consumption in underway seawater lines: Implications for air-sea O2 and CO2 fluxes', *Geophysical Research Letters*, 37(1), pp. 1–5. doi: 10.1029/2009GL040423.

Langer, G., Probert, I. and Ziveri, P. (2011) 'The morphological response of Emiliania huxleyi to seawater carbonate chemistry changes : an inter-strain comparison', 32(1), pp. 29–34.

Lee, K. *et al.* (2006) 'Global relationships of total alkalinity with salinity and temperature in surface waters of the world's oceans', *Geophysical Research Letters*, 33(19), pp. 1–5. doi: 10.1029/2006GL027207.

Liu, M. and Tanhua, T. (2019) 'Distribution of Water Masses in the Atlantic Ocean based on GLODAPv2', *Ocean Science Discussions*, (January), pp. 1–32. doi: 10.5194/os-2018-140.

Liu, M. and Tanhua, T. (2021) 'Water masses in the Atlantic Ocean: Characteristics and distributions', *Ocean Science*, 17(2), pp. 463–486. doi: 10.5194/os-17-463-2021.

Marshall, J. and Speer, K. (2012) ‘Closure of the meridional overturning circulation through Southern Ocean upwelling’, *Nature Geoscience*, 5(3), pp. 171–180. doi: 10.1038/ngeo1391.

McCartney, M.S., 1977: Subantarctic mode water, A voyage of discovery, M. Angel, Ed., Pergamon, 103-119.

McNeil, B. I. and Matear, R. J. (2008) ‘Southern Ocean acidification: A tipping point at 450-ppm atmospheric CO_2’, Proceedings of the National Academy of Sciences of the United States of America, 105(48), pp. 18860–18864. doi: 10.1073/pnas.0806318105.

Mitchell, C. *et al*. (2017) ‘Estimating Particulate Inorganic Carbon Concentrations of the Global Ocean From Ocean Color Measurements Using a Reflectance Difference Approach’, Journal of Geophysical Research: Oceans, 122(11), pp. 8707–8720. doi: 10.1002/2017JC013146.

Munro, D. R. *et al.* (2015) ‘Recent evidence for a strengthening CO2 sink in the Southern Ocean from carbonate system measurements in the Drake Passage (2002–2015)’, pp. 7623–7630. doi: 10.1002/2015GL065194.Received.

Murray, J. W. (2004) ‘The Ocean Carbon Cycle and Climate’, The Ocean Carbon Cycle and Climate, (June). doi: 10.1007/978-1-4020-2087-2.

Orsi, A. H., Whitworth, T. and Nowlin, W. D. (1995) 'On the meridional extent and fronts of the Antarctic Circumpolar Current', *Deep-Sea Research Part I*, 42(5), pp. 641–673. doi: 10.1016/0967-0637(95)00021-W.

Palter, J. B. *et al.* (2013) 'Large-Scale, Persistent Nutrient Fronts of the World Ocean: Impacts on Biogeochemistry', (August). doi: 10.1007/698_2013_241.

Raimondi, L. *et al.* (2019) 'The internal consistency of the marine carbon dioxide system for high latitude shipboard and in situ monitoring', *Marine Chemistry*. Elsevier, 213(November 2018), pp. 49–70. doi: 10.1016/j.marchem.2019.03.001.

Ren, L., Speer, K. and Chassignet, E. P. (2011) 'The mixed layer salinity budget and sea ice in the Southern Ocean', *Journal of Geophysical Research: Oceans*, 116(8), pp. 1–17. doi: 10.1029/2010JC006634.

Rokitta, S. D. (2012) 'Characterization of the life-cycle stages of the coccolithophore Emiliania huxleyi and their responses to ocean acidification ', PhD thesis(September), p. 145.

Resing, J. A. and Sansone, F. J. (1999) 'The chemistry of lava-seawater interactions: The generation of acidity', *Geochimica et Cosmochimica Acta*, 63(15), pp. 2183–2198. doi: 10.1016/S0016-7037(99)00193-3.

Riebesell, U. *et al.* (2013) 'Technical Note: A mobile sea-going mesocosm system - New opportunities for ocean change research', *Biogeosciences*, 10(3), pp. 1835–1847. doi: 10.5194/bg-10-1835-2013.

Sarmiento, J. L. *et al.* (2004) 'High-latitude controls of thermocline nutrients and low latitude biological productivity', *Nature*, 427(6969), pp. 56–60. doi: 10.1038/nature02127.

Sokolov, S. and Rintoul, S. R. (2002) 'Structure of Southern Ocean fronts at 140°E', *Journal of Marine Systems*, 37(1–3), pp. 151–184. doi: 10.1016/S0924-7963(02)00200-2.

Stark, J. S. *et al.* (2018) 'Carbonate chemistry of an in-situ free-ocean CO_2 enrichment experiment (antFOCE) in comparison to short term variation in Antarctic coastal waters', Scientific Reports. Springer US, 8(1), pp. 1–16. doi: 10.1038/s41598-018-21029-1.

Tanhua, T. *et al.* (2017) 'Temporal changes in ventilation and the carbonate system in the Atlantic sector of the Southern Ocean', *Deep-Sea Research Part II: Topical Studies in Oceanography*. Elsevier, 138, pp. 26–38. doi: 10.1016/j.dsr2.2016.10.004.

Tomczak, M. (1999) 'Some historical, theoretical and applied aspects of quantitative water mass analysis', *Journal of Marine Research*, 57(2), pp. 275–303. doi: 10.1357/002224099321618227.

Tomczak, M. and Liefrink, S. (2005) ‘Interannual variations of water mass volumes in the Southern Ocean’, *Journal of Atmospheric and Ocean Science*, 10(1), pp. 31–42. doi: 10.1080/17417530500062838.

Tynan, E. *et al.* (2016) ‘Physical and biogeochemical controls on the variability in surface pH and calcium carbonate saturation states in the Atlantic sectors of the Arctic and Southern Oceans’, *Deep-Sea Research Part II: Topical Studies in Oceanography*. Elsevier, 127, pp. 7–27. doi: 10.1016/j.dsr2.2016.01.001.

Williams, N. L. *et al.* (2018) ‘Assessment of the Carbonate Chemistry Seasonal Cycles in the Southern Ocean From Persistent Observational Platforms’, *Journal of Geophysical Research: Oceans*, 123(7), pp. 4833–4852. doi: 10.1029/2017JC012917.

Wu, Y. *et al.* (2019) ‘What drives the latitudinal gradient in open-ocean surface dissolved inorganic carbon concentration?’, *Biogeosciences*, 16(13), pp. 2661–2681. doi: 10.5194/bg-16-2661-2019.

Zeebe, R. E. and Wolf-Gladrow, D. A. (2009) ‘Carbon dioxide, dissolved (Ocean)’, Encyclopedia of Earth Sciences Series, 2(Figure 1), pp. 1037–1039. doi: 10.1007/978-1-4020-4411-3_30.